Biofuel Research Journal 43 (2024) 2168-2180

Biofuel Research Journal

Journal homepage: www.biofueljournal.com

Original Research Paper

# Sustainable catalytic pathways for biofuel precursors: quantitative conversion of glucose to gluconic acid using Pt-Zn biochar catalyst

Hengyu Hao[1], Haixin Guo[1,*], Bingkun Chen[1], Richard Lee Smith Jr[2], Feng Shen[1,*]

[1]*Agro-Environmental Protection Institute, Ministry of Agriculture and Rural Affairs, No. 31 Fukang Road, Nankai District, Tianjin 300191, China.*

[2] *Graduate School of Environmental Studies, Tohoku University, Aramaki Aza Aoba 468-1, Aoba-ku, Sendai 980-8572, Japan.*

## HIGHLIGHTS

- Pt-Zn intermetallic nanoparticle catalyst prepared via a one-pot solvothermal reaction.
- A 99.9% total selectivity was obtained in pure water in air without any additives.
- Spectroscopic analyses verified the formation of Pt-Zn intermetallic nanoparticle alloy.
- Isotope labeling confirmed gluconic acid carboxyl oxygen from the water hydroxyl group.
- Pt-Zn/strawC catalyst and competing catalysts were assessed with environmental indicators.

## GRAPHICAL ABSTRACT

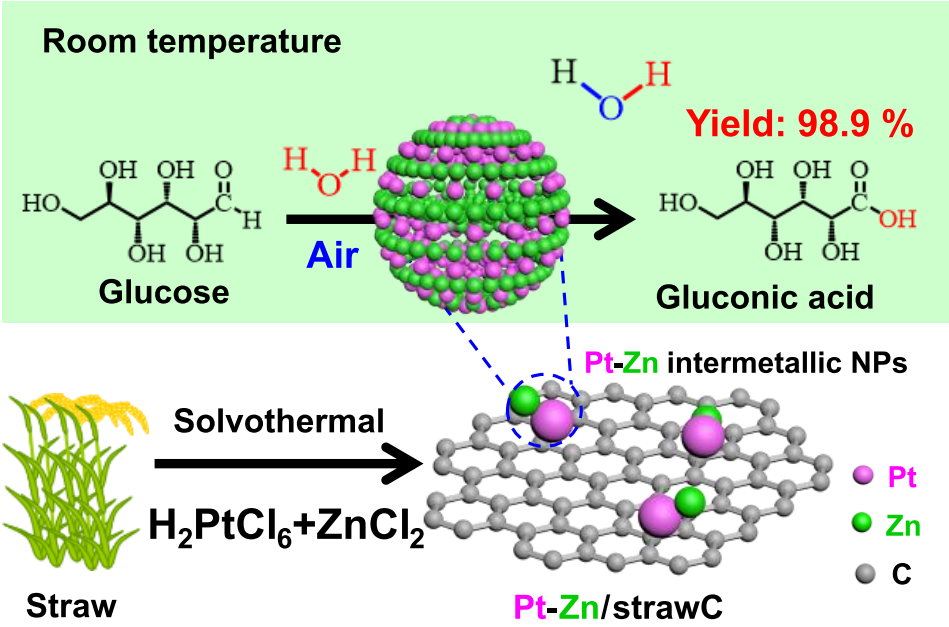


## ARTICLE INFO

**Article history:**
Received 2 May 2024
Received in revised form 11 July 2024
Accepted 1 August 2024
Published 1 September 2024

**Keywords:**
Biomass
Pt-Zn alloy
Biochar
Solvothermal synthesis
One-pot reaction
Sugar acid

## ABSTRACT

Achieving quantitative conversion of biomass-derived feedstocks under ambient environmental conditions (20°C, atmospheric air, 0.1 MPa) is a critical milestone for sustainability in chemical processes. Herein, the quantitative conversion of glucose to gluconic acid was accomplished under ambient environmental conditions without any additives using a Pt-Zn intermetallic nanoparticle-supported biochar catalyst prepared from raw rice straw (Pt-Zn/strawC) *via* a straightforward one-pot solvothermal reaction with ethylene glycol solvent. Spectroscopic analyses verified the formation of the Pt-Zn intermetallic alloy and confirmed strong electronic metal-support interactions. The Pt-Zn/strawC catalyst (Pt:Zn molar ratio of 1:6) was highly selective for the conversion of glucose to gluconic acid, whereas yields as high as 99.9% (98.9% gluconic acid, 1.0% glucaric acid) were reached at 20 °C under base-free and additive-free conditions. Isotope measurements and density functional theory revealed synergistic interactions in the Pt-Zn alloy, wherein the alloy tended to absorb glucose and active $O_2$ into superoxide radical ($O_2$·). This work demonstrates a chemocatalytic method that is practical for environmental conditions and provides a new avenue for sustainable conversion of lignocellulosic biomass to chemical products.

**©2024 Alpha Creation Enterprise CC BY 4.0**

* Corresponding authors at:
E-mail address: haixin_g@126.com; (Haixin Guo); shenfeng@caas.cn (Feng Shen)

Please cite this article as: Hao H., Guo H., Chen B., Smith Jr R.L., Shen F. Sustainable catalytic pathways for biofuel precursors: quantitative conversion of glucose to gluconic acid using Pt-Zn biochar catalyst. Biofuel Research Journal 43 (2024) 2168-2180. DOI: 10.18331/BRJ2024.11.3.3.

**Contents**



| **Abbreviations** | |
|---|---|
| DFT | Density function theory |
| EDX | Energy-dispersive X-ray spectroscopy |
| FTIR | Fourier transform infrared |
| HAADF-STEM | High-angle annular dark-field scanning TEM |
| HRTEM | High-resolution transmission electron microscopy |
| ICP-MS | Inductively coupled plasma mass spectrometry |
| $O_2$-TPD | $O_2$ temperature-programmed desorption |
| TEM | Transmission electron microscopy |
| TG-DTG | Thermogravimetry and differential thermal analysis |
| TOF | Turnover frequency |
| XPS | X-ray photoelectron spectroscopy |
| XRD | X-ray diffraction |
| **Nomenclature** | |
| Pt | Platinum |
| $r_0$ | Initial weight-specific activity |
| Zn | Zinc |
| **Symbols** | |
| strawC | Biochar derived from raw rice straw carbon |

## 1. Introduction

The catalytic conversion of biomass feedstocks necessitates sustainable strategies for the synthesis of organic acids (Qin et al., 2022). Considering that lignocellulose biomass derived from agricultural wastes is generated at about 181.5 billion tonnes annually (Singh et al., 2022), there are more than ample amounts of these residues for developing new feedstocks. Monosaccharides can be obtained from cellulose and hemicellulose by acid hydrolysis, in which oxidization of the aldehyde group at C1 generates sugar acids (Meng et al., 2020; Zhang et al., 2022). Sugar acids and their salts are important chemicals in health care and industrial fields, and they are essential additives in many food products (Khawaji et al., 2019).

Current industrial production of sugar acids is primarily through enzymatic oxidation of monosaccharides, although this method has inherent issues with separations, waste disposal, enzyme recycling, loss, and cost (Zhang and Huber, 2018). The development of heterogeneous catalytic oxidation systems that selectively oxidize monosaccharides in aqueous feedstocks with either air or molecular oxygen is attractive for the production of sugar acids on a large scale because issues inherent in enzymatic methods can be overcome (Deng et al., 2023).

Previous reports on heterogeneous metal catalysts have demonstrated superior oxidation activity for monosaccharides, although most studies use $O_2$ or $H_2O_2$ as an oxidant with applied pressure under conditions of elevated temperature (Zhang et al., 2022). Catalysts proposed that use Ni or Pt as active sites have been found to accelerate the oxidation of glucose by electrocatalytic and photocatalytic methods (Tian et al., 2023; Medrano-Banda et al., 2024). Noble metal Pd-modified carbons in alkaline environments can promote the oxidation of monosaccharides into sugar acids at near-room temperatures without the need for current or light control (Liu et al., 2018). **Table 1** summarizes oxidation methods for glucose according to reaction conditions and medium. Considering the progress made in glucose oxidation catalysis, it is interesting to explore whether metal-supported carbons could be developed for promoting thermo-catalytical glucose oxidation at room temperature without any additives. Especially, such evaluations of heterogeneous catalysts in the absence of additives or temperature- or pressure-related stimuli have seldomly been targeted in the literature (**Table 1**) which is the motivation for the present research.

The use of a transition metal with noble metal as an alloy is a win-win strategy in heterogeneous catalyst design because the transition metal acts to control catalyst selectivity while reducing catalyst cost (Wang et al., 2023). Among the different bimetallic systems, zinc has attracted a great deal of attention for promoting depolymerization of biomass (Pereira Lopes and Astruc, 2021) and for moderating the catalytic activity of Pt-containing catalysts (Chan et al., 2020). Synthesis of bimetallic alloy catalysts has been reported *via* stepwise preparation of support and subsequent loading of metal precursors and post-treatment methods (Yin et al., 2018; Luo et al., 2022). Luo et al. (2022) prepared Pt-Ni bimetallic nanoparticles supported on carbon *via* ultrasonication with a one-step solvothermal approach and found that the materials had high activity for promoting glycerol oxidation. Lee et al. (2008) obtained Au-Pd alloy nanoparticles *via* co-reduction of $HAuCl_4$ and $K_2PdCl_4$ *via* ascorbic acid as a reducing agent with stabilizing agents. In considering the design of bimetallic alloy catalysts, biomass residues in the form of biochars could be attractive because biochars contain a number of functional groups that can be used to interact with substrates and products.

Rice straw, which contains cellulose (24%), hemicellulose (28%), lignin (13%), and large amounts of inorganic compounds (e.g., $SiO_2$), is readily available at low cost (Rosado et al., 2022) and can be used to prepare biochars. In this work, the activity of Pt-Zn alloys having biochar supports is explored because biochars have a rich number of functional groups that offer not only control of substrate adsorption and product desorption but also have numerous binding sites and defects that may be used advantageously to mimic enzymes for promoting transformations at near-room temperature conditions.

Pt-Zn intermetallic nanoparticle supported biochar (Pt-Zn/strawC) was prepared from rice straw *via* one-pot solvothermal reduction of $PtCl_6^{2-}/Zn^{2+}$ precursors in ethylene glycol for the purpose of designing a glucose to gluconic acid oxidation catalyst. In the synthesis scheme, ethylene glycol served as a carbonization solvent for the rice straw and as a reducing agent for the $PtCl_6^{2-}/Zn^{2+}$ precursors. Biochar catalysts were prepared using

Please cite this article as: Hao H., Guo H., Chen B., Smith Jr R.L., Shen F. Sustainable catalytic pathways for biofuel precursors: quantitative conversion of glucose to gluconic acid using Pt-Zn biochar catalyst. Biofuel Research Journal 43 (2024) 2168-2180. DOI: 10.18331/BRJ2024.11.3.3.

**Table 1.**
Previously reported heterogenous catalytic glucose oxidation strategies and developed glucose oxidation method of this work.

| Entry | Catalyst | Reaction Conditions (°C/$p_{O2}$ MPa) | Additives Used in Water | Oxidation Method | Ref. |
|---|---|---|---|---|---|
| 1 | $Au_{61}Pd_{39}$/Ce-NR | 80/0.6 | 0.03 M NaOH | Thermocatalysis | Khawaji et al. (2021) |
| 2 | Ni-NCNT | 80/2 | 0.06 M $NaHCO_3$ | Thermocatalysis | Li et al. (2021a) |
| 3 | CuBC600N | 160/- | 30 wt% $H_2O_2$ | Thermocatalysis | Zhang et al. (2022) |
| 4 | Pd/CNT-N | 30/1 | 0.08 M NaOH | Thermocatalysis | Li et al. (2021b) |
| 5 | Pd/C | 25/0.1 | 0.1 M $Na_2CO_3$ | Thermocatalysis | Liu et al. (2018) |
| 6 | $Ni_{ED}$/XC72 | 25/- | 0.1 M NaOH | Electrocatalysis | Medrano-Banda et al. (2024) |
| 7 | Pt/def-$TiO_2$ | 20/- | 1 M KOH | Photoelectrocatalysis | Tian et al. (2023) |
| 8 | Pt-Zn/strawC | 20/Air | None | Thermocatalysis | **Present Study** |

(Pt:Zn) ratios ranging from 1:1 to 1:6 and blank materials were prepared using (Pt:Zn) ratios of (1:0), (0:1) and (0:0). Biochar catalysts were characterized with transmission electron microscopy (TEM), high-resolution TEM (HRTEM), high-angle annular dark-field scanning TEM (HAADF-STEM), X-ray photoelectron spectroscopy (XPS), X-ray diffraction (XRD), energy-dispersive X-ray spectroscopy (EDX), Raman spectroscopy, Fourier transform infrared (FTIR) spectroscopy, inductively-coupled plasma mass spectroscopy (ICP-MS), and oxygen temperature programmed desorption ($O_2$-TPD). Oxygen isotope analyses were used to elucidate the role of oxidation active sites of the biochar catalysts and the mechanism of glucose to gluconic acid transformation.

## 2. Experimental

### *2.1. Materials*

Chloroplatinic acid (99.995%) was purchased from Aladdin (China). Zinc chloride (99%), glucose (99%), and ethylene glycol (98%) were obtained from Macklin (China). Water used in the experiments was obtained with a purification apparatus (Merck Millipore SYPK0SIX2). All chemicals were used as received without further purification. Rice straw used in preparing the biochars was obtained from Dali city (Yunnan, China). The rice straw was washed with water, dried at 60 °C for 12 h, and characterized by the thermogravimetry and differential thermogravimetry (TG-DTG) method.

### *2.2. Catalyst preparation*

Pt-Zn alloy-supported biochars were prepared from raw rice straw with solvothermal carbonization using ethylene glycol solvent and $H_2PtCl_6$ as Pt precursor and $ZnCl_2$ as Zn precursor. The raw straw and $ZnCl_2$ (mass ratio of 1:1) were pretreated by ball milling (PM100, Retsch, Germany) for 1 h at 350 rpm and room temperature conditions. Generally, 0.8 g ball-milling power, 0.2 g $H_2PtCl_6$ (Zn:Pt molar ratio of 6), 0.2 g NaOH, and 20 mL ethylene glycol were added to a Teflon stainless-steel autoclave (100 mL), and heated at 195 °C. After 12 h, the resulting solid was separated by centrifugation, washed five times with ethanol and water, and oven-dried at 80 °C for 12 h.

The resulting powder from the above procedure is designated as Pt-Zn/strawC, with a molar ratio of Pt to Zn in the synthesis of 1:6. Pt-Zn(1:x)/strawC was prepared using Pt:Zn molar ratios of (1:x) under identical conditions. Blanks designated as Pt/strawC and Zn/strawC were prepared by excluding $ZnCl_2$ or $H_2PtCl_6$ while performing identical processing steps. Another blank designated as strawC was prepared by using raw rice straw without metals that was directly carbonized with NaOH in ethylene glycol after ball milling.

### *2.3. Characterization methods*

The as-prepared materials were characterized with TEM (Thermo Fisher Talos F200s) at 200 kV. Samples for TEM measurements were prepared by transferring solutions diluted with ethanol onto a copper grid. XRD (Rigaku Ultima IV) was performed to identify the crystal structure of catalysts using Cu Kα radiation (40 kV, 40mA) within a 2θ range from 5° to 90° (scanned at 8°·min$^{-1}$). Analysis of functional groups on the materials was performed with Raman spectroscopy (Thermo Fisher DXRxi) at 633 nm excitation and FTIR spectroscopy (Tianjin Nengpu iCAN 8 Plus) after mixing samples with KBr powder as the matrix. XPS was performed with a Thermo ESCALAB 250XI instrument using a monochromatic Al Kα X-ray source with a pass energy of 20 eV and 200 scans. Metal content was analyzed with ICP-MS using an Agilent 7850 instrument. The oxidation capacity of the samples was determined with a Tianjin Xianquan TP-5080 $O_2$-TPD instrument. Spectrometry analyses for isotope-labeled compounds were carried out with a ZenoTOF 7600 (Sciex, USA) instrument. TG-DTG curves were measured with a thermal analysis system (Netzsch STA449 F5) in which samples were under a nitrogen atmosphere and subjected to a temperature profile of (25 to 500) °C at a heating rate of 10 °C·min$^{-1}$.

### *2.4. Catalytic performance and analytical methods*

Catalytic oxidation reactions of glucose to D-gluconic acid were carried out in 20 mL Teflon stainless-steel autoclaves. Generally, 0.05 g of glucose, 0.02 g of catalyst, and 5 mL of water were added into the autoclaves and heated and stirred by a controller (HA-5 Haian Petroleum Scientific Research Instrument Co., Ltd.). After a given time, the solution was separated by filtration (0.2 μm, polyethersulfone membrane) and analyzed with high-performance liquid chromatography (Waters e2489) with an Aminex HPX-87H column at 50 °C using $H_2SO_4$ (5mM) (0.6 mL·min$^{-1}$) as mobile phase and analyte detection by refractive index and ultraviolet absorption. Solids were washed with ethanol and water four times, dried overnight in a vacuum oven, and the catalyst was either analyzed or used in the next run. Glucose conversion, D-gluconic acid yield, and turnover frequency (TOF) were calculated by **Equations 1-3**:

$$\text{Conversion (mol\%)} = \left(1-\frac{\text{moles of sugar in the product}}{\text{initial moles of the substrate}}\right) \times 100 \quad \text{Eq.1}$$

$$\text{Yield (mol\%)} = \left(\frac{\text{moles of sugar acid in the product}}{\text{initial moles of the substrate}}\right) \times 100 \quad \text{Eq.2}$$

$$\text{TOF} = \frac{\text{number of glucose molecules converted by catalyst per unit time}}{\text{number of surface Pt sites}} = \frac{\frac{r_0 \times M_{Pt}}{\text{Pt loading} \times \text{Pt dispersion}}}{} \ (h^{-1}) \quad \text{Eq.3}$$

where $r_0$ represents initial weight-specific activity and $M_{Pt}$ stands for molar mass of Pt. Calculation details of $r_0$ and TOF are provided in the **Supplementary Material** (**Fig. S1**).

Please cite this article as: Hao H., Guo H., Chen B., Smith Jr R.L., Shen F. Sustainable catalytic pathways for biofuel precursors: quantitative conversion of glucose to gluconic acid using Pt-Zn biochar catalyst. Biofuel Research Journal 43 (2024) 2168-2180. DOI: 10.18331/BRJ2024.11.3.3.

## 3. Results and Discussion

### *3.1. Characterization*

The morphologies of the as-prepared materials were examined using TEM (**Figs. 1a-c**). Pt-Zn/strawC (**Fig. 1a**) shows finely dispersed particles in the nanometer range with a porous appearance, whereas Zn/strawC (**Fig. 1b**) and Pt/strawC (**Fig. 1c**) exhibit agglomerated particles ranging from 3 to 6.5 nm in diameter. From the TEM results, it is likely that the presence of Zn promoted the dispersion of Pt in the carbon structure. EDX with elemental mapping showed that C, N, and O were finely distributed in the solid, and Pt and Zn were dispersed (**Fig. 1d**). The TEM-EDX element atomic image of Pt-Zn/strawC showed low silicon content (**Fig. S2**). TG-DTG curves of straw after ball milling revealed that there was little or no mineral in the processed Pt-Zn/strawC sample (**Fig. S3**). HAADF-STEM image analysis of Pt-Zn/strawC exhibited that its spherical-like clusters had diameters of approximately 1.6 nm (**Fig. 1e**). An HRTEM image of Pt-Zn/strawC (**Fig. 1f**) revealed an interplanar distance of about 0.27 nm and 0.22 nm for the Pt–Zn alloy corresponding to lattice spacing of the $Pt_3Zn$ (110) (Zakaria et al., 2021) and (111) (Luo et al., 2022) planes, respectively (Kang et al., 2012). The metallic content of Pt-Zn/strawC samples was determined by ICP-MS (**Table S1**), and a 4:1 stoichiometric ratio for Pt:Zn was revealed, indicating the presence of Pt–Zn alloy and a small amount of free Pt, thus confirming intermetallic nanoparticles. Platinum content in the as-prepared Pt/strawC samples was 12.1 $mg \cdot g^{-1,}$ and zinc content in the as-prepared Zn/strawC samples was 16.9 $mg \cdot g^{-1}$.

**Figure 2a** shows XRD patterns of the as-prepared metal-supported biochars. All samples displayed peaks at about 15.9° and 22.5°, which are assigned to the (101) and (002) planes of cellulose (Lei et al., 2022). Compared with strawC biochar, peaks of cellulose for the metal-supported biochar became weaker. For bimetallic-supported biochar Pt-Zn/strawC, diffraction peaks at 18.9° are assigned to semicrystalline hemicellulose (Louis et al., 2020). The broad peak of Pt-Zn/strawC at approximately 38° is related to the (100) crystal plane of disordered carbon (Jiang et al., 2019), which suggests that platinum and zinc metals exist in an amorphous region of the biochar in the samples prepared at Pt:Zn molar ratios of (1:6) and (1:1).

For Zn/strawC, diffraction peaks at 31.9°, 34.7°, 36.4°, 47.6°, 56.8°, 63.0°, and 68.2° are attributed to (100), (002), (101), (102), (110), (103), and (112) of ZnO corresponding to the rutile phase (PDF#36-1451) (Arun et al., 2022). For Pt/strawC biochar, diffraction peaks at 40.1°, 46.5°, 67.8°, 81.6°, and 86.2° are assigned to Pt (111), Pt (200), Pt (220), Pt (311), and Pt

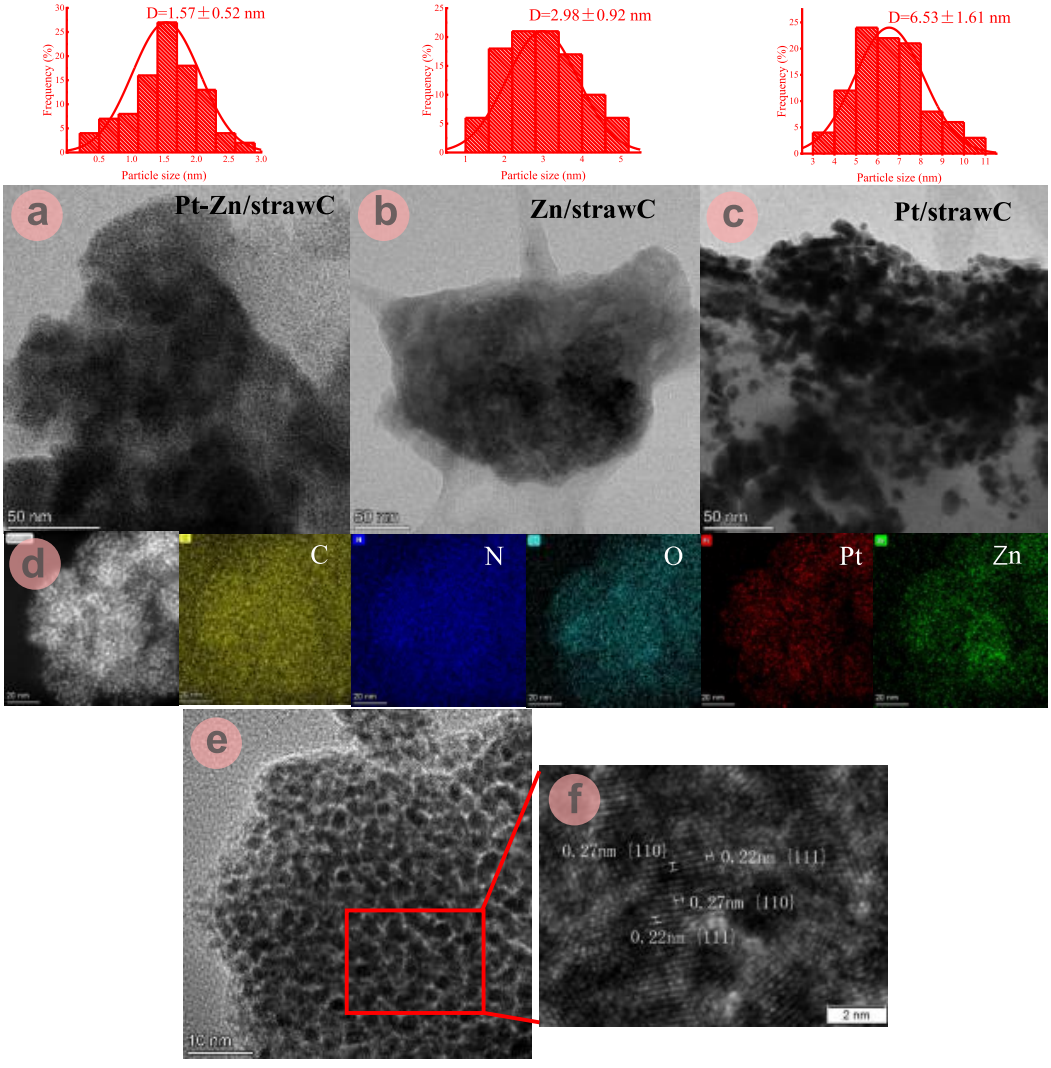


**Fig. 1.** Structural characterization of Pt-Zn/strawC, Zn/strawC, and Pt/strawC: **(a-c)** TEM images; **(d)** HAADF-STEM and EDX element mapping image; and **(e-f)** HRTEM image of spherical Pt–Zn alloy of Pt-Zn/strawC (Yellow: carbon, Navy blue: nitrogen, Blue: oxygen, Red: platinum, and Green: zinc).

Please cite this article as: Hao H., Guo H., Chen B., Smith Jr R.L., Shen F. Sustainable catalytic pathways for biofuel precursors: quantitative conversion of glucose to gluconic acid using Pt-Zn biochar catalyst. Biofuel Research Journal 43 (2024) 2168-2180. DOI: 10.18331/BRJ2024.11.3.3.

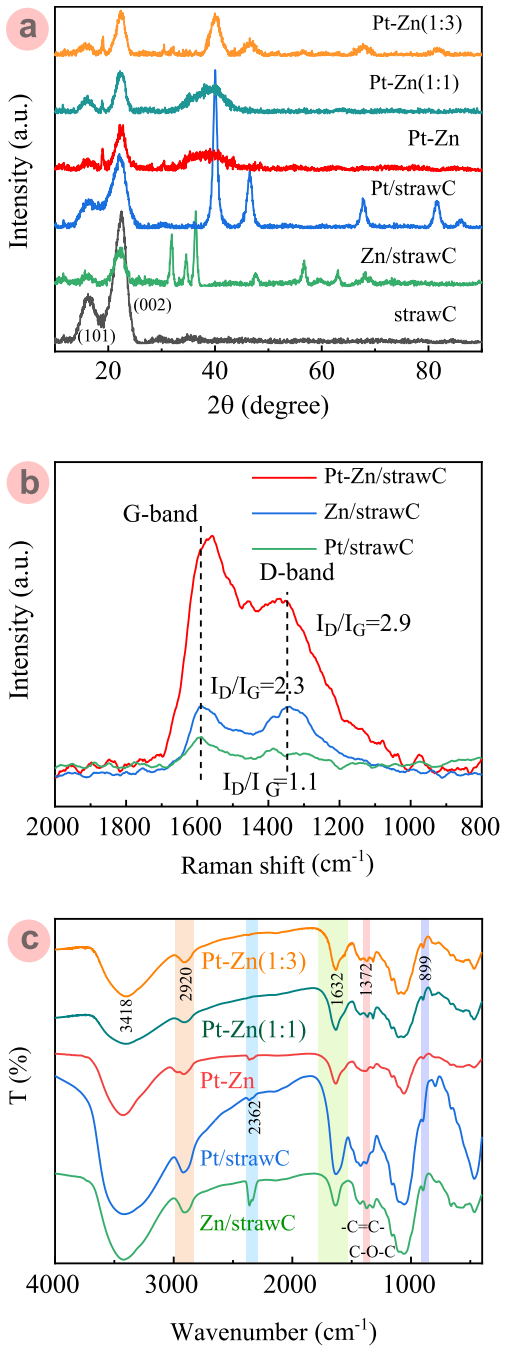


**Fig. 2.** Analyses of as-prepared Pt and Zn containing biochar (/strawC) materials: **(a)** XRD; **(b)** Raman spectra; and **(c)** FTIR spectra.

(222), respectively, corresponding to a face-centered cubic (fcc) structure (Liu et al., 2023). For Pt-Zn/strawC, no diffraction peaks associated with Pt or Zn metal were observed, whereas diffraction peaks at 40.0°, 46.5°, 67.8°, and 81.6° corresponding to free Pt were only found in Pt-Zn(1:3)/strawC samples, which may be attributed to low concentrations and well-dispersed Pt and Zn nanoparticles on the surfaces of the other samples (Sun et al., 2022).

Two characteristic Raman peaks of 1347 $cm^{-1}$ and 1590 $cm^{-1}$ were observed for all biochars, which are attributed to the D and G bands, respectively (Meng et al., 2020). The intensity ratios of these two peaks ($I_D/I_G$) of the as-prepared samples (**Fig. 2b**) showed that Pt-Zn/strawC had a higher $I_D/I_G$ value (2.9) compared with those of Zn/strawC (2.3) or Pt/strawC (2.1) samples, which can be attributed to the smaller crystallite sizes of Pt-Zn alloys (Mori et al., 2018). Metal atoms, especially the Pt atom, have a large effect on the graphitization of amorphous carbon (Tang et al., 2013) and seem to be related to bonds between carbon in the sp2 hybrid configuration of graphite being destroyed to form oxygen-containing functional groups (C-O, COOH) that leads to an increase in disordered carbon (Kim et al., 2014).

The functional groups of all biochars were characterized by FTIR (**Fig. 2c**), wherein the wide transmission peak at approximately 3418 $cm^{-1}$ is attributed to OH bond stretching (Fang et al., 2022) and peaks at 1632 $cm^{-1}$ and 1372 $cm^{-1}$ are attributed to N-H and COOH stretching (Li et al., 2021b), while vibrations of amorphous cellulose at around 2920 $cm^{-1}$ and 899 $cm^{-1}$ are typical bands probably originating from the stretching of single bond C-H in saturated fatty hydrocarbons in straw (Do Nascimento et al., 2019; Jiang et al., 2019). The relative intensity of the C≡N (2362 $cm^{-1}$) bond (Zakaria et al., 2021) of Pt-Zn/strawC and Zn/strawC samples was higher than that of other samples. Considering the results given by Raman spectroscopy (**Fig. 2b**), zinc most likely promoted the carbonization of the straw, resulting in the formation of C≡N bonds.

Molar ratios of Pt:Zn and surface composition of oxygen for the materials are given in **Table S2**. The higher Pt:Zn molar ratio of the Pt-Zn/strawC sample over those in either the Pt-Zn(1:3)/strawC or Pt-Zn(1:1)/strawC samples implies high metal surface concentration. Moreover, XPS measurements confirmed that the content of Pt and Zn atoms on the surface of Pt-Zn/strawC material was almost equal (**Table S2**), which was consistent with EDX elemental mapping results (**Fig. S2**). In the XPS survey spectra, Pt, Zn, O, C, and N were clearly observed in the Pt-Zn/strawC sample compared with the other samples (**Fig. S4**). High-resolution Pt 4f core-level XPS spectrum of Pt-Zn/strawC were deconvoluted into dominating metallic state $Pt^0$, where the binding energies of $Pt^0$ for Pt-Zn/strawC samples were determined to be 75.5 eV and 72.2 eV (**Fig. 3a**), which was higher than values reported for $Pt^0$ as bare Pt in metallic foil of 74.4 eV and 71.1 eV, respectively (Hagiwara et al., 2013), meaning that surface electrons of $Pt^0$ in the Pt-Zn/strawC sample had been transferred. The shift of binding energies could be attributed to existing interactions between Pt and the carbon support (Zhao et al., 2023). The Zn 2p spectra of Pt-Zn/strawC samples had typical ZnO profiles (**Fig. 3b**), in which the binding energy peaks for Pt-Zn/strawC were located at 1045.3 eV (Zn 2p1/2) and 1022.2 eV (Zn 2p3/2) corresponding to a distinctive peak separation of ZnO (23.1 eV) (Tu et al., 2017). The binding energy of Zn for the Pt-Zn/strawC sample was shifted by about 0.3 eV positively compared with ZnO, indicating that surface electrons of Zn in Pt-Zn alloy had probably been redistributed (Zhao et al., 2023). The presence of strong electronic metal-support interactions in the Pt-Zn/strawC effectively modulated the electronic structure of the PtZn alloy nanoparticle and led to its improved catalytic properties.

The $Pt^0$ (or ZnO) shift relative to bare Pt foil (or pure ZnO) decreased with decreasing Pt/Zn molar ratio on the surface (**Figs. 3a** and **3b**). The XPS spectrum for Pt/strawC sample could be deconvoluted into $Pt^0$ and $Pt(OH)_2$, respectively (**Fig. 3a**). The binding energy of Zn 2p spectrum in Zn/strawC sample at 1046.5 eV and 1023.4 eV both shifted to values that were about 1.5 eV higher than those of pure ZnO (**Fig. 3b**), revealing that atomic electrons of Zn were transferred to the support (Zhao et al., 2023). The O 1s spectrum could be deconvoluted into lattice oxygen $O^{2-}$ from ZnO, oxygen-deficient regions, and absorbed oxygen species from OH (**Fig. 3c**). Compared with Pt/strawC, the amount of OH oxygen species in the oxygen vacancies for the Pt-Zn/strawC and Zn/strawC samples increased due to the introduction of Zn (**Table S2**).

The type and mobility of oxygen species of the samples were studied with $O_2$-TPD (**Fig. 3d**) that showed desorption peaks below 200 °C, which could be attributed to weakly chemisorbed oxygen ($O^{2-}$, $O_2^{2-}$ or $O^-$) (Yang et al., 2020). The $O_2$-TPD profiles for Pt-Zn/strawC, Zn/strawC, and Pt/strawC samples showed the presence of chemically-adsorbed species at around 167 °C, 196 °C, and 221 °C (**Fig. 3d**), which can be attributed to surface-active oxygen ($O^{2-}$, $O_2^{2-}$ or $O^-$) (Yang et al., 2020). The starting temperature of the lowest desorption peak for the Pt-Zn/strawC sample occurred at a lower temperature than either the Pt/strawC or Zn/strawC samples, implying that the Pt-Zn/strawC sample had higher catalytic activity than the single metal samples (Ma et al., 2010).

Please cite this article as: Hao H., Guo H., Chen B., Smith Jr R.L., Shen F. Sustainable catalytic pathways for biofuel precursors: quantitative conversion of glucose to gluconic acid using Pt-Zn biochar catalyst. Biofuel Research Journal 43 (2024) 2168-2180. DOI: 10.18331/BRJ2024.11.3.3.

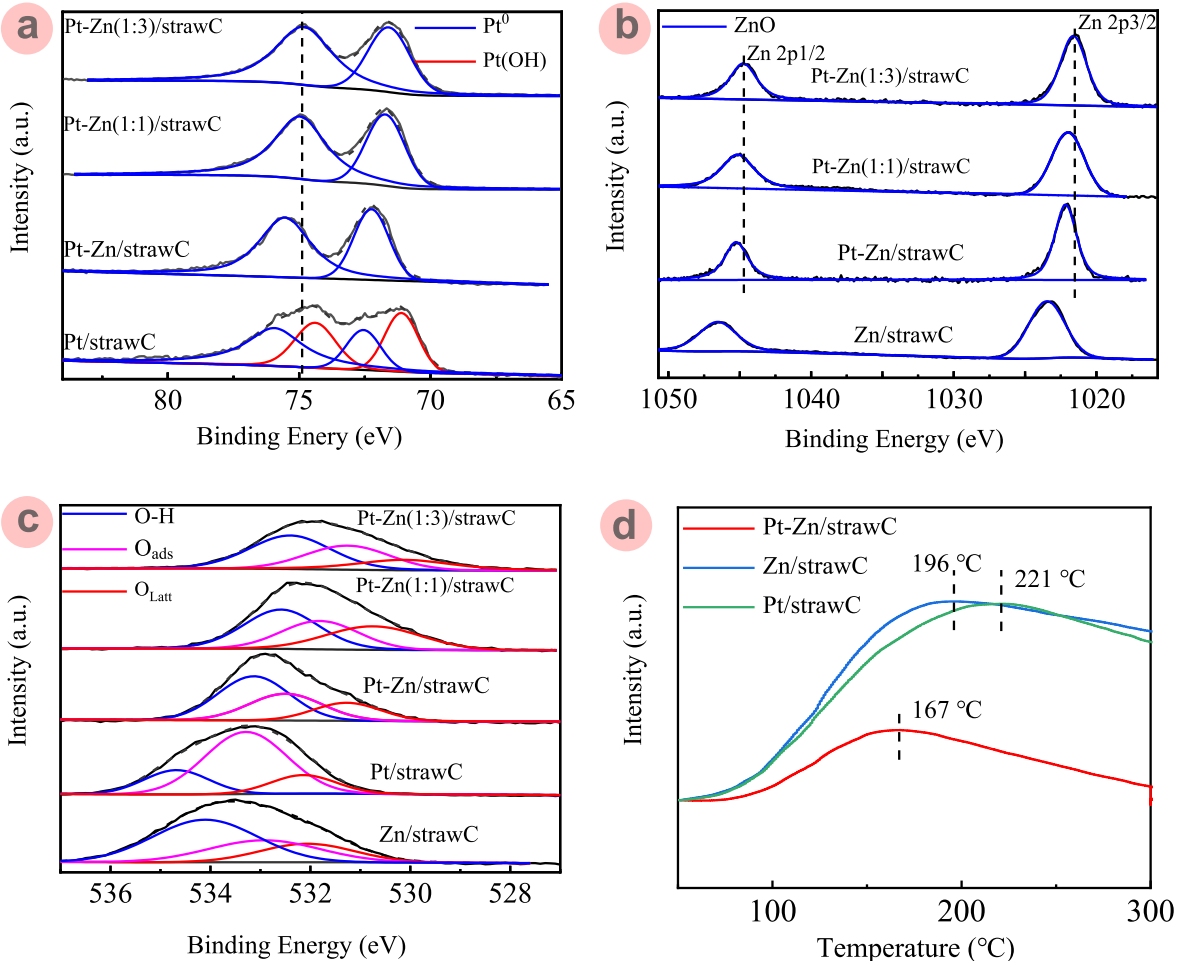


**Fig. 3.** Characteristics of Pt-Zn/strawC, Pt/strawC, and Zn/strawC materials: **(a)** XPS Pt 4f spectra; **(b)** XPS Zn 2p spectra; **(c)** XPS O 1s spectra; and **(d)** $O_2$-TPD profiles for as-prepared Pt-Zn/strawC material (red line); Zn/strawC material (blue line); Pt/strawC material (green line).

The corresponding structural evolution of the prepared Pt-Zn alloy materials can be summarized according to the above analyses (**Scheme 1**). Functional carbon substrate formed in one pot from rice straw *via* solvothermal carbonization in an ethylene glycol solution that contained Pt and Zn precursors. A neutralization reaction took place with the addition of NaOH into the $H_2Pt_4Cl_6$ precursor solution that reacted to form Pt complexes as $[Pt(OH)_6]^{2-}$ until all $Cl^-$ ions were replaced by $OH^-$ ions (Zeng et al., 2020). The $OH^-$ ions precipitated as Pt (IV) onto the carbon substrate (Qi et al., 2017). Under reducing conditions originating from ethylene glycol, $Pt^{4+}$ with its lower reduction potential, was preferentially reduced to form Pt nanoparticles (Yu et al., 2013; Zeng et al., 2020). As a parallel reaction, ZnO particles were converted into hydro-complexes $Zn(OH)_2$ in ethylene glycol solution from released $Zn^{2+}$ ions. Under a reducing environment promoted by solvothermal conditions, reduction of $Pt^{4+}$ occurred near the Zn nanoparticles to form Pt-Zn alloys on the functional carbon substrates.

### *3.2. Catalytic activity*

The as-prepared materials were applied as catalysts for promoting glucose oxidation (**Table 2**), wherein control experiments without the addition of a catalyst gave low glucose conversions (1.8%) and no gluconic acid formation (*Entry 1*, **Table 2**). When Zn/strawC catalyst was applied (*Entry 2*, **Table 2**), glucose conversion increased over experiments performed without a catalyst; however, gluconic acid was still not detected, which can be attributed partly to the oxidation of zinc and formation of ZnO phases in the catalyst (Potter et al., 2012). When the Pt/strawC catalyst was employed (*Entry 3*, **Table 2**), glucose conversion increased over the value obtained for the Zn/strawC catalyst, and a 21% yield of gluconic acid was obtained. Furthermore, when the Pt-Zn/strawC catalyst was applied (*Entry 4*, **Table 2**), glucose conversion increased to 100% and afforded a gluconic acid yield of 87.6%. According to $r_0$ and Pt dispersion, the TOF for Pt-Zn/strawC catalyst (*Entry 4*, **Table 2**) was determined to be 4819 $h^{-1}$, which was much higher than reported TOF values for Pd/C (TOF: 859.7 $h^{-1}$) (Liu et al., 2018).

Since reaction systems with the Pt-Zn/strawC catalyst were not optimized, some attempts were made at changing conditions such as substrate concentrations, reaction temperatures, and oxygen partial pressures (*Entries 8-9*, **Table 2**) that were chosen to be similar to those used in literature studies (*Entries 6-7*, **Table 2**), where it was found that relatively high glucose conversions (>90%) could be obtained (*Entries 8-9*, **Table 2**); however, the gluconic acid yields became lower than 73% indicating a decrease in selectivity.

To examine possible structure-activity relationships, Zn content was lowered from (1:6) used in preparing Pt-Zn/strawC samples (*Entry 4*, **Table 2**) to (mol:mol) ratios of (1:3) or (1:1) as shown in **Table 2** (*Entries 10-13*). Comparing the samples prepared at the Pt:Zn ratio of 1:6 (*Entry 4*, **Table 2**) with other preparation variations (*Entries 11* and *13*, **Table 2**) at the same reaction conditions, it can be seen that glucose conversions were 100%, and gluconic acid yields were similar for all materials, although slightly lower

Please cite this article as: Hao H., Guo H., Chen B., Smith Jr R.L., Shen F. Sustainable catalytic pathways for biofuel precursors: quantitative conversion of glucose to gluconic acid using Pt-Zn biochar catalyst. Biofuel Research Journal 43 (2024) 2168-2180. DOI: 10.18331/BRJ2024.11.3.3.

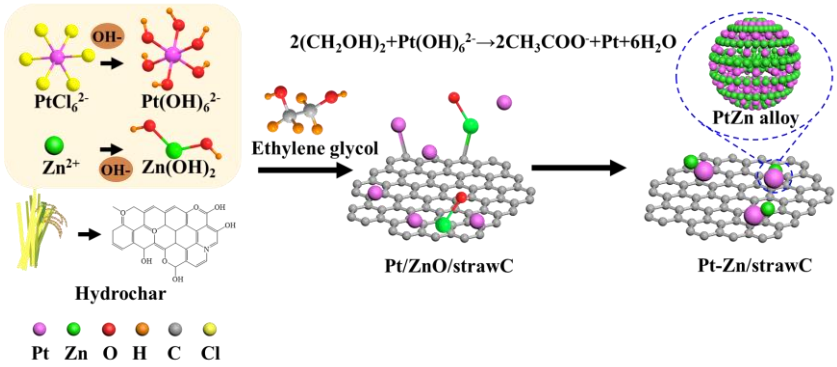


**Scheme 1.** Schematic illustration of intermetallic Pt-Zn/strawC material formation.

**Table 2.**
Oxidation of glucose (Glu) to gluconic acid in water with as-prepared materials applied as catalysts (Cat) in the presence of gas atmospheres having partial pressure (*p*). Partial pressures in reaction systems are 1 MPa unless otherwise specified.

| Entry | Catalyst | Reaction System | | | *T* (°C) | Tim (h) | *P* (MPa) | Conversion (%) | Product Yields (%) | | | Ref. |
|---|---|---|---|---|---|---|---|---|---|---|---|---|
| | | Glu (g) | Glu (g) | Glu (g) | | | | | Gluconic Acid | Gluconic Acid | Total | |
| 1 | - | 0.05 | 0.02 | 5 | 100 | 1.5 | $O_2$ | 1.8 | - | - | - | * |
| 2 | Zn/strawC | 0.05 | 0.02 | 5 | 100 | 1.5 | $O_2$ | 4.2 | - | - | - | * |
| 3 | Pt/strawC | 0.05 | 0.02 | 5 | 100 | 1.5 | $O_2$ | 28.7 | 21.0 | 0.2 | 21.2 | * |
| 4 | Pt-Zn/strawC | 0.05 | 0.02 | 5 | 100 | 1.5 | $O_2$ | 100 | 87.6 | 3.8 | 91.4 | * |
| 5[a] | Pt/HT | 0.7 | 0.3 | 30 | 50 | 12 | $O_2$, 0.1 MPa | 99.0 | 83.0 | - | 83.0 | Tathod et al. (2014) |
| 6[b] | Pd/CNT-N | 0.15 | $3.6 \cdot 10^{-5}$ | 25 | 30 | 3 | $O_2$ | 99.4 | 98.3 | - | 98.3 | Li et al. (2021b) |
| 7 | Pd/CNT-N | 0.15 | $3.6 \cdot 10^{-5}$ | 25 | 30 | 3 | $O_2$ | 5.4 | 0.9 | - | 0.9 | Li et al. (2021b) |
| 8 | Pt-Zn/strawC | 0.15 | 0.004 | 25 | 30 | 3 | $O_2$ | 94.8 | 44.1 | 0.6 | 44.7 | * |
| 9 | Pt-Zn/strawC | 0.05 | 0.02 | 5 | 30 | 3 | $O_2$ | 90.5 | 73.0 | 0.8 | 73.8 | * |
| 10 | Pt-Zn (1:3)/strawC | 0.05 | 0.02 | 5 | 100 | 1 | $O_2$ | 100 | 80.3 | 1.4 | 81.7 | * |
| 11 | Pt-Zn (1:3)/strawC | 0.05 | 0.02 | 5 | 100 | 1.5 | $O_2$ | 100 | 83.1 | 2.2 | 85.3 | * |
| 12 | Pt-Zn (1:1)/strawC | 0.05 | 0.02 | 5 | 100 | 1 | $O_2$ | 100 | 85.3 | 2.9 | 88.2 | * |
| 13 | Pt-Zn (1:1)/strawC | 0.05 | 0.02 | 5 | 100 | 1.5 | $O_2$ | 100 | 87.5 | 3.3 | 90.8 | * |
| 14 | Pt-Zn/strawC | 0.05 | 0.02 | 5 | 20 | 72 | Air, 0.1 MPa | 100 | 98.9 | 1.0 | 99.9 | * |
| 15 | Pt-Zn/strawC | 0.05 | 0.02 | 5 | 100 | 1.5 | $N_2$ | 48.1 | 46.6 | - | 45.6 | * |
| 16 | Pt/straw | 0.05 | 0.02 | 5 | 100 | 1.5 | $N_2$ | 7.1 | 3.7 | - | 3.7 | * |
| 17 | Zn/straw | 0.05 | 0.02 | 5 | 100 | 1.5 | $N_2$ | 2.6 | - | - | - | * |
| 18[c] | Pt-Zn/strawC | 0.05 | 0.02 | 5 | 100 | 1.5 | $N_2$ | 15.8 | 15.2 | - | 15.2 | * |
| 19[c] | Pt-Zn/strawC | 0.05 | 0.02 | 5 | 20 | 72 | $N_2$ | 39.7 | 35.7 | 0.6 | 36.3 | * |

*Present study: [a] 63 mmol/L of Na2CO3 added to reaction system; [b] 80 mmol/L of NaOH added to reaction system; [c] water degassed by boiling to remove dissolved oxygen before use.

yields were observed for the Pt-Zn (1:3)/strawC catalyst (*Entry 11*, Table 2) that may be related to free Pt metal on the biochar as evident from the lack of a Pt-Zn amorphous region at around 40° in the XRD pattern of Pt-Zn (1:3)/strawC material (Fig. 2a). For a given Pt:Zn preparation ratio (*Entries 10-11* or *12-13*, Table 2), increasing reaction time from 1 to 1.5 h led to an increase in both gluconic acid and glucaric acid yields and a corresponding decrease in selectivity implying that some amount of gluconic acid ($C_6H_{12}O_7$) was oxidized to glucaric acid ($C_6H_{10}O_8$). According to these experimental results (*Entries 1-13*, Table 2), the presence of Zn with Pt in the biochars enhanced selectivity for glucose oxidation in all prepared samples, whereas lower amounts of free Pt metal in the biochar seemed to be favorable for improving glucose oxidation.

From the results shown for Pt-Zn/strawC catalysts (*Entries 8-9*, Table 2), glucose oxidation selectivity increased at 30 °C compared with reactions at 100 °C and required longer reaction times as expected. Motivated by this trend, an experiment was performed at ambient conditions for long reaction times (*Entry 14*, Table 2), wherein remarkably, 100% glucose conversion was obtained at 72 h in air with 98.9% glucose oxidation selectivity (=98.9/100.0) (TOF: 82 $h^{-1}$). To explore the reason for the high selectivity of Pt-Zn/strawC catalysts for glucose oxidation, additional experiments were performed in the presence of nitrogen (*Entries 15-19*, Table 2), in which two experiments were performed under anaerobic conditions. With the Pt-Zn/strawC catalyst, glucose oxidation proceeded with high selectivity. Compared with anaerobic conditions, the yield of gluconic acid increased to about 31.4% in which the consumption of active oxygen (0.087

Please cite this article as: Hao H., Guo H., Chen B., Smith Jr R.L., Shen F. Sustainable catalytic pathways for biofuel precursors: quantitative conversion of glucose to gluconic acid using Pt-Zn biochar catalyst. Biofuel Research Journal 43 (2024) 2168-2180. DOI: 10.18331/BRJ2024.11.3.3.

mmol) was equated with dissolved oxygen in the water at 100 ºC and is known to be about 0.097 mmol (Galamba et al., 2019). Thus, the presence of some amount of oxygen is key to applying the Pt-Zn/strawC catalyst at ambient conditions, and therefore, the $^{18}O$ experiments were performed to elucidate the mechanism, as discussed later.

### *3.3. Oxidation of glucose at room temperature*

The effect of reaction time on the oxidation of glucose over the as-prepared Pt-Zn intermetallic nanoparticle biochar catalyst is presented in **Figure 4**. As shown, an 87.2% conversion of glucose and 80.5% yield of gluconic acid were obtained in 24 h. The yield of gluconic acid increased to a maximum of 98.9% when the reaction time was prolonged from 24 to 72 h. Further prolonging the reaction time to 120 h led to the conversion of some amounts of gluconic acid into glucaric acid (9%) (**Fig. 4**).

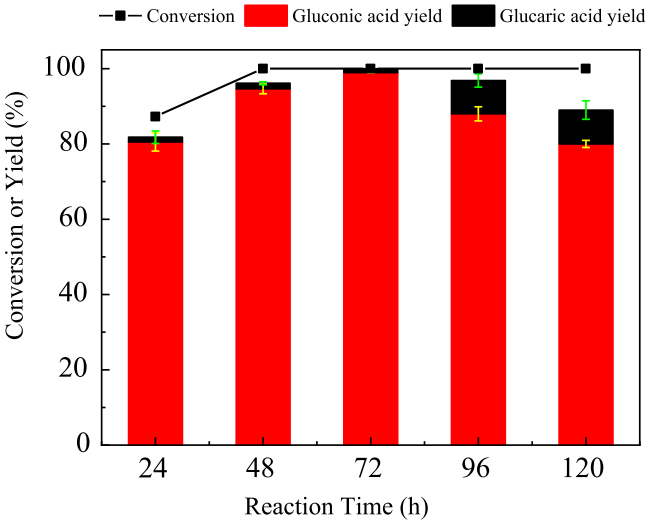


**Fig. 4.** Oxidation of glucose with as-prepared Pt-Zn intermetallic nanoparticle biochar catalyst (Pt-Zn/strawC) at room temperature (*Reaction conditions:* 0.05 g of substrate, 0.02 g of catalyst, 5 mL water, 20 ºC, in the presence of atmospheric air).

### *3.4. Optimization of reaction conditions*

Based on the above experimental results, the reaction system using the Pt-Zn/strawC catalyst was optimized for gluconic acid yield (**Figs. 5a-b**) at temperatures from 90 to 110 ºC in an attempt to shorten reaction time. Glucose conversion and gluconic acid yield increased as reaction temperature was increased for 0.5 h reaction time. When the reaction temperature was increased from 100 to 110 ºC, gluconic acid yield decreased from 87.6 to 80.7% due to by-product formation of acetic acid. At 1 h reaction time, both glucose conversion and gluconic acid yields increased at each reaction temperature examined. The gluconic acid yield reached 87.6% with glucose conversion up to 100% at 100 ºC for a 1.5 h reaction, in which the gluconic acid yield decreased to 73.1% after a 4 h reaction time. Results were consistent with a previous report that found gluconic acid to be unstable at high temperatures and long reaction times that promote further oxidation of gluconic acid (Li et al., 2021a).

It has been reported that $O_2$ is critical for aerobic oxidation of monosaccharides (Zhang and Huber, 2018). About 36.6% of glucose was transformed over Pt-Zn/strawC catalyst (**Fig. 5c**), whereas only less oxidized products (gluconic acid, 31.8%) were obtained without the addition of $O_2$. In general, reaction conditions of monosaccharides to sugar acids are favored under aerobic environments (Qi et al., 2022). After the reactor was purged with pure oxygen several times and the corresponding $O_2$ partial pressure was maintained, gluconic acid yields increased with an increase in $O_2$ partial pressure from 0.2 to 1 MPa (**Fig. 5c**). Among the glucose oxidation trials with $O_2$ addition, the highest gluconic acid yield was obtained at an $O_2$ partial pressure of 1 MPa. When the $O_2$ partial pressure was increased to 1.8 MPa, yields of gluconic acid decreased to 71.2%, which infers that excess oxygen in the reaction system resulted in product oxidation (Li et al., 2021a).

The influence of the amount of catalyst on the oxidation performance of glucose was also investigated (**Fig. 5d**). The oxidation of glucose to gluconic acid did not occur in the absence of catalyst (**Fig. 5d**). Gluconic acid yields increased when the catalyst was used (5 mg), suggesting that the Pt-Zn/strawC catalyst was active for the oxidation of glucose. Glucose conversions and gluconic acid yields increased to their highest values among the trials of 100% and 87.6%, respectively, when the amount of catalyst was increased from 5 to 20 mg. When 30 mg of catalyst was used, overoxidation occurred, and a 75.7% yield of gluconic acid was obtained for 100% glucose conversion.

### *3.5. Reaction mechanism*

Glucose oxidation over the Pt-Zn/strawC catalyst was monitored with isotopic labeling of $H_2{}^{18}O$ in which the incorporation of $^{18}O$ into gluconic acid was observed (**Fig. 6a**). The mass-to-charge ratio (m/z) at 195 and 197 represented $^{16}O$-containing and $^{18}O$-containing gluconic acid; thus, it can be suggested that glucose reacts with hydroxide ions that dissociate from water to form the carboxyl oxygen source of gluconic acid over Pt-Zn/strawC catalyst (**Fig. 6b**). Incorporation of $^{18}O$ into gluconic acid can be attributed to favorable active sites of Pt-Zn intermetallic nanoparticles in the biochar catalyst. A proper amount of $O_2$ allows selective oxidation of glucose to gluconic acid. One possible role of $O_2$ is that it acts as an electron scavenger to remove protons from H-metal intermediates to regenerate the catalyst *in situ* (Zhou et al., 2019).

Density function theory (DFT) calculations were performed on theoretical structures representing Pt/strawC, Zn/strawC, and Pt-Zn/strawC materials (**Supplementary Materials**). As shown in **Figure 7**, the adsorption energies of Pt (111), ZnO (101), and $Pt_3Zn$ (111) for glucose were -1.34, -2.11, and -1.45 eV, respectively, and corresponding desorption energies were 1.39, 4.53, and 1.45 eV, suggesting that glucose adsorption is favored over glucose desorption for the catalytic materials. Desorption energies of gluconic acid on Zn/strawC material were higher than those on Pt-Zn/strawC material, indicating favorable product desorption.

A plausible reaction mechanism for glucose oxidation over Pt-Zn intermetallic nanoparticle catalyst can be proposed (**Scheme 2**). Pt-Zn intermetallic nanoparticles act as active sites and, with water as the nucleophile, adsorb glucose to form intermediate **1** and subsequent dehydrogenation to give **2**. Gluconic acid is formed by the dissociation of the formyl C-H bond of **2**, followed by a hydrogen shift with the release of one molecule of water. The surface of the metal Pt-Zn intermetallic nanoparticles preferably attracts the CHO side-chain of glucose while hydroxide ions dissociate from water.

### *3.6. Recycling and reuse*

The stability and reusability of the as-prepared Pt-Zn/strawC was studied (**Fig. S5a**). The glucose conversion remained (>99%) almost unchanged after four runs at identical reaction conditions (**Fig. S5a**). However, gluconic acid yields decreased from 98.9 to 80.9% after four times use (**Fig. S5a**) but showed that the Pt-Zn/strawC catalyst was recyclable under reaction conditions. Reaction solutions of each run were analyzed with ICP-MS and showed ppm levels of metal inferring that undue metals were not leached from the catalyst at reaction conditions. XPS spectra Pt 4f and O 1s for the spent catalyst were similar to those of the fresh catalyst (**Figs. 3a-c** and **Figs. S5b-d**), suggesting that the lower gluconic acid yields observed in the recycling experiments could be attributed to changes in Pt/Zn molar ratio of the surface (*Entry 6*, **Table S2**). It can be speculated that gluconic acid yield decreased with reuse primarily due to the reduction in the adsorption of substrate. FTIR analyses of the spent catalysts showed that the peak of CO shifted to higher wavenumbers and new peaks at CONH (1719 $cm^{-1}$) and $CO_3^{2-}$ (1426 $cm^{-1}$) were observed (**Fig. 2c** and **Fig. S6**), suggesting that the as-prepared Pt-Zn/strawC catalyst acted as oxygen precursor in glucose conversion to gluconic acid under nitrogen atmosphere conditions.

Please cite this article as: Hao H., Guo H., Chen B., Smith Jr R.L., Shen F. Sustainable catalytic pathways for biofuel precursors: quantitative conversion of glucose to gluconic acid using Pt-Zn biochar catalyst. Biofuel Research Journal 43 (2024) 2168-2180. DOI: 10.18331/BRJ2024.11.3.3.

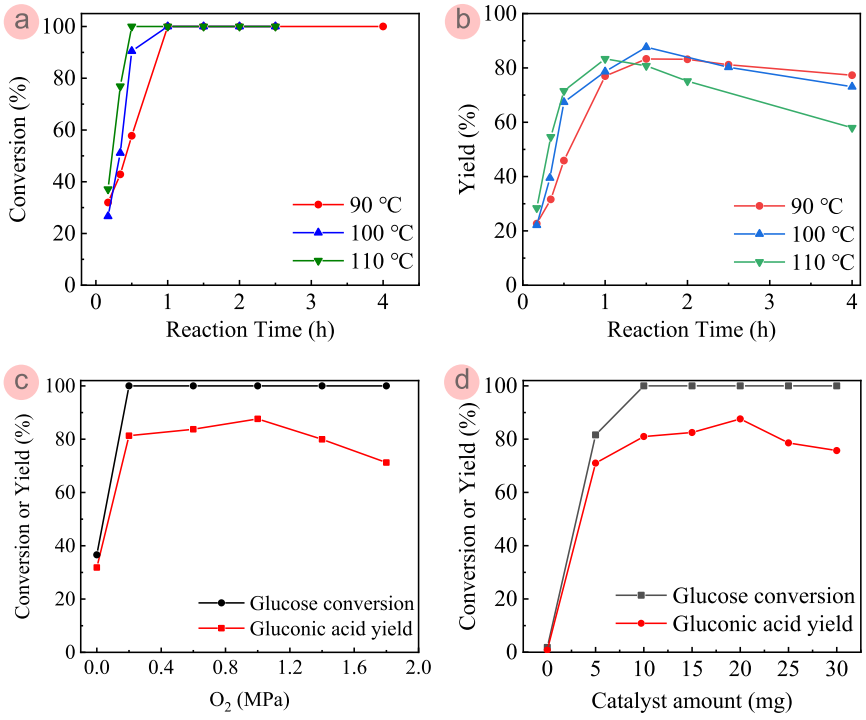


**Fig. 5.** The reaction results for oxidation of glucose over Pt-Zn/strawC catalyst: **(a)** glucose conversion versus reaction time at 90 to 110 °C and **(b)** gluconic acid yield versus reaction time at 90 to 110 °C (*Reaction conditions:* 0.05 g of glucose, 0.02 g of catalysts, 5 mL water, 1 MPa $O_2$, 800 rpm). Glucose conversion or gluconic acid yield versus: **(c)** oxygen partial pressure (*Reaction conditions:* 0.05 g of glucose, 0.02 g of catalysts, 5 mL water, 100 °C, 1.5 h, 800 rpm.); and **(d)** catalyst amount (*Reaction conditions:* 0.05 g of glucose, 5 mL water, 1 MPa $O_2$, 100 °C, 1.5 h, 800 rpm).

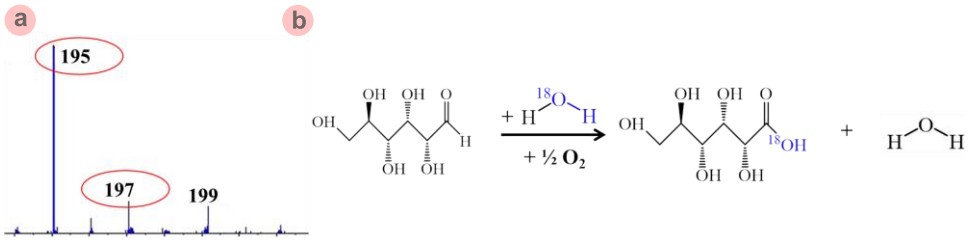


**Fig. 6.** Reaction with $^{18}O$ labeled reagents: **(a)** mass spectra of gluconic acid from glucose oxidation; **(b)** carboxyl oxygen source of gluconic acid in the reaction system. Experiments with isotopes were carried out at 20 °C for 72 h under atmospheric air conditions without additives (*Reaction conditions:* 0.05 g glucose, 0.02 g Pt-Zn/strawC catalyst, and 1 mL $H_2{}^{18}O$ added to 4 mL $H_2{}^{16}O$ solvent).

### *3.7. Techno-economic analysis*

The catalytic oxidation process of glucose reactions was assessed using several key indicators, including process efficiency, catalyst cost, energy consumption, oxidant cost, environmental benefits, and cycling performance (**Table S3**). The indicators used were normalized for comparison purposes, with highly favorable performance assigned to a value of 5, unfavorable performance assigned a value of 1, and values between 1 and 5 used for intermediate performance (Yadav et al., 2023). **Figure 8** presents a radar map for comparing catalysts proposed for the oxidation of glucose. The catalyst in this work was prepared using platinum and raw rice straw, which reduces production cost compared with catalysts that use noble metals or carbon sources such as carbon nanotubes as raw materials (**Table S3**). For process efficiency, the yield and selectivity of sugar acids reached 99.9%, which is higher than that of reported catalysts. In terms of energy consumption, the oxidation experiment progresses at room temperature without electricity or the involvement of light or photons. With the exception of air, oxidants or alkali additives are not required to promote glucose oxidation, which reduces costs and is environmentally friendly.

## 4. Challenges and Perspectives

To achieve sustainable production of gluconic acid, heterogeneous catalysts are expected to replace enzymes and homogeneous catalysts presently being used for industrial oxidation of glucose. It has been reported that alkaline solutions are a critical requirement for a good number of catalysts; however, this research points to completely different avenues, namely, that glucose oxidation can occur without the presence of a base. Therefore, it is important to focus on the development of heterogeneous catalysts that can be used under base-free conditions, which will avoid wastewater generation, equipment corrosion, and numerous post-treatment steps.

Although the Pt-Zn/strawC catalyst designed in this work is shown to have high activity in aqueous solutions, Pt-transition metal alloy catalysts perform with higher recyclability and at a lower cost than single precious metal catalysts. Future studies may pay more attention to reducing the

Please cite this article as: Hao H., Guo H., Chen B., Smith Jr R.L., Shen F. Sustainable catalytic pathways for biofuel precursors: quantitative conversion of glucose to gluconic acid using Pt-Zn biochar catalyst. Biofuel Research Journal 43 (2024) 2168-2180. DOI: 10.18331/BRJ2024.11.3.3.

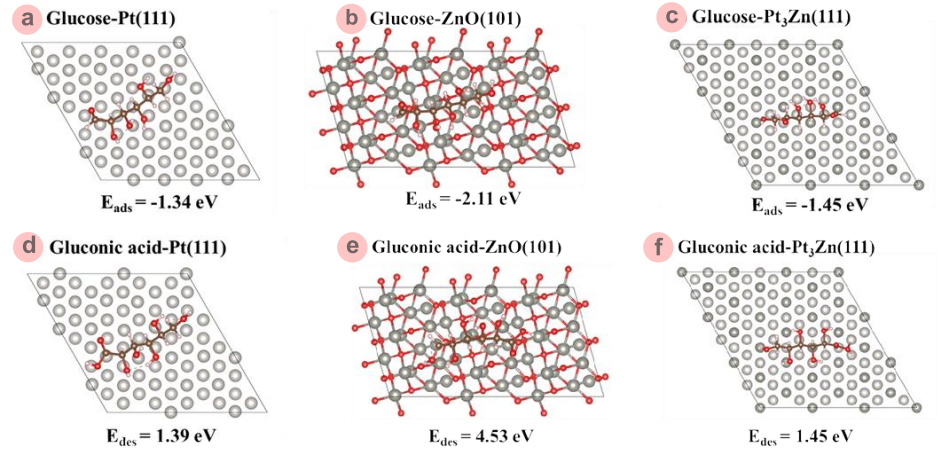


**Fig. 7.** Glucose adsorption (ads) energies and gluconic acid desorption (des) energies calculated with density function theory (DFT) for graphene layers representing Pt/strawC, Zn/strawC, and Pt-Zn/strawC catalytic materials: **(a)** glucose-graphene-Pt (111); **(b)** glucose-graphene-ZnO (101); **(c)** glucose-graphene-$Pt_3Zn$ (111); **(d)** gluconic acid-graphene-Pt (111); **(e)** gluconic acid-graphene-ZnO (101); and **(f)** gluconic acid-graphene-$Pt_3Zn$ (111).

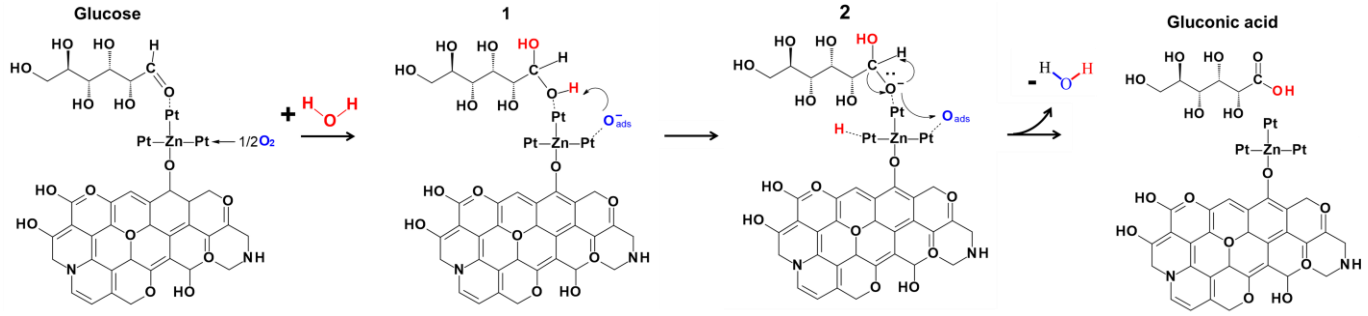


**Scheme 2.** Proposed reaction mechanism for the oxidation of glucose to gluconic acid over Pt-Zn intermetallic nanoparticle catalyst (Pt-Zn/strawC).

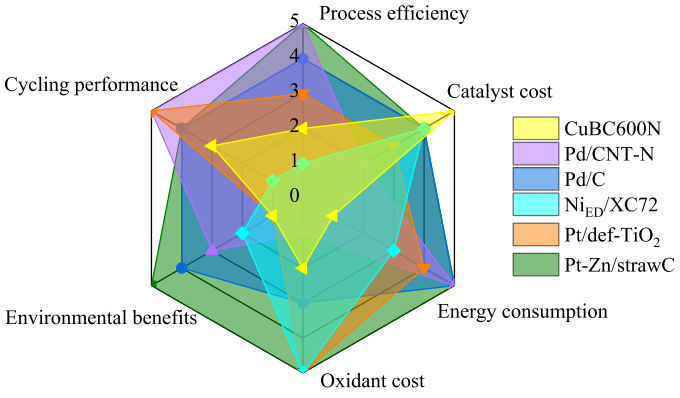


**Fig. 8.** Radar map for comparing heterogeneous catalysts for oxidation of glucose according to indicators: process efficiency, catalyst cost, energy consumption, oxidant cost, environmental benefits, and cycling performance.

amount of precious metal or in the design of catalytic systems for other oxidation reactions to improve sustainability. From the viewpoint of industrial application, biochar is highly suited as a support or carrier for active metals because it provides active oxygenated sites that affect oxidation progress, and there can be many unique combinations depending on the source of lignocellulose as raw material.

It is noteworthy that the industry tends to develop continuous reactions for mass production. The Pt-Zn/strawC catalyst demonstrated in this work can simplify catalytic conversions under base-free conditions by reducing environmental pollution and by using sustainable processing conditions. Before practical scaled-up applications can be realized, however, there must be the design of process flowsheets with appropriate heat transfer, mass transfer, and separation operations, each of which requires further investigation. Nevertheless, there will be a great need for biochar catalysts that are able to effectively promote reactions without additives in environmental conditions.

Please cite this article as: Hao H., Guo H., Chen B., Smith Jr R.L., Shen F. Sustainable catalytic pathways for biofuel precursors: quantitative conversion of glucose to gluconic acid using Pt-Zn biochar catalyst. Biofuel Research Journal 43 (2024) 2168-2180. DOI: 10.18331/BRJ2024.11.3.3.

## 5. Conclusions

In this work, the quantitative conversion of glucose to gluconic acid was achieved with a Pt-Zn intermetallic nanoparticle catalyst prepared from raw rice straw (Pt-Zn/strawC). The PtZn intermetallic nanoparticles were confirmed by HRTEM and XPS analyses. Due to bimetallic synergy and the presence of strong electronic metal-support interactions, the Pt-Zn/strawC catalyst (Pt:Zn molar ratio of 1:6) was highly selective for sugar acid generation from glucose at room temperature under base-free conditions without any additives and at atmospheric air conditions. Isotope labeling experiments confirmed that the carboxyl oxygen of gluconic acid was mainly derived from the dissociated hydroxyl group in water. Experimental isotope measurements showed the detailed mechanism in which the selectivity of the Pt-Zn intermetallic nanoparticles for glucose oxidation can be attributed to interactions between Pt and Zn as an alloy. The present research provides a sustainable pathway for the production of high-value-added sugar acids from monosaccharides at room temperature and atmospheric air conditions. Before practical scaled-up processes can be realized, further investigations are needed on the heat and mass transfer of product separation.

## Acknowledgments

The authors are grateful for the Elite Youth program of the Chinese Academy of Agricultural Sciences (to Haixin Guo), Key Laboratory of Technologies and Models for Cyclic Utilization from Agricultural Resources, Ministry of Agriculture and Rural Affairs, P. R. China (KLTMCUAR2023-02), and the Central Public-interest Scientific Institution Basal Research Fund (No. Y2022QC30).

## References

[1] Arun, V., Manikandan, V., Alsalhi, M.S., Devanesan, S., Priyadharsan, A., Kumar, K.A.R., Maadeswaran, P., 2022. An efficient optical properties of Sn doped ZnO/CdS based solar light driven nanocomposites for enhanced photocatalytic degradation applications. Chemosphere. 300, 134460-134468.

[2] Chan, Y.T., Siddharth, K., Shao, M., 2020. Investigation of cubic Pt alloys for ammonia oxidation reaction. Nano Res. 13(7), 1920-1927.

[3] Deng, W., Feng, Y., Fu, J., Guo, H., Guo, Y., Han, B., Jiang, Z., Kong, L., Li, C., Liu, H., Nguyen, P.T.T., Ren, P., Wang, F., Wang, S., Wang, Y., Wang, Y., Wong, S.S., Yan, K., Yan, N., Yang, X., Zhang, Y., Zhang, Z., Zeng, X., Zhou, H., 2023. Catalytic conversion of lignocellulosic biomass into chemicals and fuels. Green Energy Environ. 8(1), 10-114.

[4] Do Nascimento, E.S., Pereira, A.L.S., Barros, M.D.O., Barroso, M.K.D.A., Lima, H.L.S., Borges, M.D.F., Feitosa, J.P.D.A., De Azeredo, H.M.C., Rosa, M.D.F., 2019. TEMPO oxidation and high-speed blending as a combined approach to disassemble bacterial cellulose. Cellulose. 26(4), 2291-2302.

[5] Fang, Y., Shu, C., Yang, L., Xue, C., Luo, P., Xu, X., 2022. Preparation and properties of magnesium cement-based photocatalytic materials. Catalysts. 12(4), 420-430.

[6] Galamba, N., Paiva, A., Barreiros, S., Simoes, P., 2019. Solubility of polar and nonpolar aromatic molecules in subcritical water: the role of the dielectric constant. J. Chem. Theory comput. 15(11), 6277-6293.

[7] Hagiwara, H., Nagatomo, M., Seto, C., Ida, S., Ishiahara, T., 2013. Dye modification effects on TaON for photocatalytic hydrogen production from water. Catalysts. 3(3), 614-624.

[8] Jiang, W., Xing, X., Li, S., Zhang, X., Wang, W., 2019. Synthesis, characterization and machine learning based performance prediction of straw activated carbon. J. Clean. Prod. 212, 1210-1223.

[9] Kang, Y., Pyo, J.B., Ye, X., Gordon, T.R., Murray, C.B., 2012. Synthesis, shape control, and methanol electro-oxidation properties of Pt-Zn alloy and $Pt_3Zn$ intermetallic nanocrystals. ACS Nano. 6(6), 5642-5647.

[10] Khawaji, M., Zhang, Y., Loh, M., Graça, I., Ware, E., Chadwick, D., 2019. Composition dependent selectivity of bimetallic Au-Pd NPs immobilised on titanate nanotubes in catalytic oxidation of glucose. Appl. Catal., B. 256, 117799-117811.

[11] Khawaji, M., Graça, I., Ware, E., Chadwick, D., 2021. Catalytic oxidation of glucose over highly stable $Au_xPd_y$ NPs immobilised on ceria nanorods. Catal. Today. 365, 257-264.

[12] Kim, T.H., Jeon, E.K., Ko, Y., Jang, B.Y., Kim, B.S., Song, H.K., 2014. Enlarging the d-spacing of graphite and polarizing its surface charge for driving lithium ions fast. J. Mater. Chem. A. 2(20), 7600-7605.

[13] Lee, Y.W., Kim, N.H., Lee, K.Y., Kwon, K., Kim, M., Han, S.W., 2008. Synthesis and characterization of flower-shaped porous Au-Pd alloy nanoparticles. J. Phys. Chem. C. 112(17), 6717-6722.

[14] Lei, W., Pei, H., Fang, C., Zhou, X., Zhang, X., Pu, M., 2022. Influence of nanocrystalline cellulose extracted from different precursors on properties of polyurethane elastomer composites. Compos. Sci. Technol. 218, 109159-109166.

[15] Li, Z., Li, D., Ma, J., Zou, R., Li, X., Liu, C., Peng, X., 2021a. Highly selective oxidation of monosaccharides to sugar acids by nickel-embedded carbon nanotubes under mild conditions. Renewable Energy. 175, 650-659.

[16] Li, Z., Li, D., Lan, W., Li, X., Wan, X., Sun, R., Liu, C., Peng, X., 2021b. Highly selective oxidation of monosaccharides to sugar acids at room temperature over palladium supported on surface functionalized carbon nanotubes. Green Chem. 23(18), 7084-7092.

[17] Liu, A., Huang, Z., Wang, X., 2018. Efficient oxidation of glucose into gluconic acid catalyzed by oxygen-rich carbon supported Pd under room temperature and atmospheric pressure. Catal. Lett. 148(7), 2019-2029.

[18] Liu, S., Jiang, Y., Wang, M., Huan, Y., He, Y., Cheng, Q., Cheng, Y., Liu, J., Zhou, X., Qian, T., Yan, C., 2023. Awakening (220) as one more active facet of PtMo alloy via single-atom doping to boost ammonia electrooxidation in direct ammonia fuel cell. Adv. Funct. Mater. 33(47), 2306204 -2306213.

[19] Louis, A.C.F., Venkatachalam, S., 2020. Energy efficient process for valorization of corn cob as a source for nanocrystalline cellulose and hemicellulose production. Int. J. Biol. Macromol. 163, 260-269.

[20] Luo, H., Yukuhiro, V.Y., Fernandez, P.S., Feng, J., Thompson, P., Rao, R.R., Cai, R., Favero, S., Haigh, S.J., Durrant, J.R., Stephens, I.E.L., Titirici, M.M., 2022. Role of Ni in PtNi bimetallic electrocatalysts for hydrogen and value-added chemicals coproduction via glycerol electrooxidation. ACS Catal. 12(23), 14492-14506.

[21] Ma, C.Y., Mu, Z., Li, J.J., Jin, Y.G., Cheng, J., Lu, G.Q., Hao, Z.P., Qiao, S.Z., 2010. Mesoporous $Co_3O_4$ and $Au/Co_3O_4$ catalysts for low-temperature oxidation of trace ethylene. J. Am. Chem. Soc. 132(8), 2608-2613.

[22] Medrano-Banda, A., Ginoux, E., Faverge, T., Oshchepkov, A., Bonnefont, A., Chatenet, M., Coutanceau, C., Kéranguéven, G., Cognet, P., Savinova, E., 2024. Electrochemical oxidation of glucose in alkaline environment-a comparative study of Ni and Au electrodes. Electrochim. Acta. 487, 144159.

[23] Meng, X., Li, Z., Li, D., Huang, Y., Ma, J., Liu, C., Peng, X., 2020. Efficient base-free oxidation of monosaccharide into sugar acid under mild conditions using hierarchical porous carbon supported gold catalysts. Green Chem. 22(8), 2588-2597.

[24] Mori, F., Kubouchi, M., Arao, Y., 2018. Effect of graphite structures on the productivity and quality of few-layer graphene in liquid-phase exfoliation. J. Mater. Sci. 53(18), 12807-12815.

[25] Pereira Lopes, R., Astruc, D., 2021. Biochar as a support for nanocatalysts and other reagents: recent advances and applications. Coord. Chem. Rev. 426, 213585-213621.

[26] Potter, M.E., Paterson, A.J., Raja, R., 2012. Transition metal versus heavy metal synergy in selective catalytic oxidations. ACS Catal. 2(12), 2446-2451.

[27] Qi, X., Fu, J., Jiang, K., Chen, T., He, Y., Li, J., Cao, J., Wei, H., Huang, L., Chu, H., 2022. Suppressing catalyst deactivation on $Pd/CeO_2$ for selective oxidation of glucose into gluconic acid. J. Catal. 414, 44-52.

[28] Qi, Z., Xiao, C., Liu, C., Goh, T.W., Zhou, L., Maligal-Ganesh, R., Pei, Y., Li, X., Curtiss, L.A., Huang, W., 2017. Sub-4 nm PtZn intermetallic nanoparticles for enhanced mass and specific activities

Please cite this article as: Hao H., Guo H., Chen B., Smith Jr R.L., Shen F. Sustainable catalytic pathways for biofuel precursors: quantitative conversion of glucose to gluconic acid using Pt-Zn biochar catalyst. Biofuel Research Journal 43 (2024) 2168-2180. DOI: 10.18331/BRJ2024.11.3.3.

in catalytic electrooxidation reaction. J. Am. Chem. Soc. 139(13), 4762-4768.
[29] Qin, N., Wu, X., Liu, X., Xue, Z.H., Muddassir, M., Sakiyama, H., Xia, C., Zhang, C., Zhu, L., Ke, F., 2022. Well-arranged hollow Au@Zn/Ni-MOF-2-$NH_2$ core-shell nanocatalyst with enhanced catalytic activity for biomass-derived d-xylose oxidation. ACS Sustainable Chem. Eng. 10(17), 5396-5403.
[30] Rosado, M.J., Marques, G., Rencoret, J., Gutiérrez, A., Del Río, J.C., 2022. Chemical composition of lipophilic compounds from rice (oryza sativa) straw: a n attractive feedstock for obtaining valuable phytochemicals. Front. Plant Sci. 13, 868319-868330.
[31] Singh, N., Singhania, R.R., Nigam, P.S., Dong, C.D., Patel, A.K., Puri, M., 2022. Global status of lignocellulosic biorefinery: challenges and perspectives. Bioresour. Technol. 344, 126415.
[32] Sun, M., Zhang, Y., Liu, W., Zhao, X., Luo, H., Miao, G., Wang, Z., Li, S., Kong, L., 2022. Synergy of metallic Pt and oxygen vacancy sites in Pt-$WO_{3-x}$ catalysts for efficiently promoting vanillin hydrodeoxygenation to methylcyclohexane. Green Chem. 24(24), 9489-9495.
[33] Tang, J., Wang, T., Sun, X., Guo, Y., Xue, H., Guo, H., Liu, M., Zhang, X., He, J., 2013. Effect of transition metal on catalytic graphitization of ordered mesoporous carbon and Pt/metal oxide synergistic electrocatalytic performance. Microporous Microporous Mater. 177, 105-112.
[34] Tathod, A., Kane, T., Sanil, E.S., Dhepe, P.L., 2014. Solid base supported metal catalysts for the oxidation and hydrogenation of sugars. J. Mol. Catal. A: Chem. 388-389, 90-99.
[35] Tian, Z., Da, Y., Wang, M., Dou, X., Cui, X., Chen, J., Jiang, R., Xi, S., Cui, B., Luo, Y., Yang, H., Long, Y., Xiao, Y., Chen, W., 2023. Selective photoelectrochemical oxidation of glucose to glucaric acid by single atom Pt decorated defective $TiO_2$. Nat. Commun. 14(1).
[36] Tu, Z., Yang, G., Song, H., Wang, C., 2017. Amorphous ZnO quantum dot/mesoporous carbon bubble composites for a high-performance lithium-Ion battery anode. ACS Appl. Mater. Interfaces. 9(1), 439-446.
[37] Wang, J., Pan, F., Chen, W., Li, B., Yang, D., Ming, P., Wei, X., Zhang, C., 2023. Pt-based intermetallic compound catalysts for the oxygen reduction reaction: structural control at the atomic scale to achieve a win-win situation between catalytic activity and stability. Electrochem. Energy Rev. 6(1).
[38] Yadav, G., Singh, A., Dutta, A., Uekert, T., Desveaux, J.S., Nicholson, S.R., Tan, E.C.D., Mukarakate, C., Schaidle, J.A., Wrasman, C.J., Carpenter, A.C., Baldwin, R.M., Román-Leshkov, Y., Beckham, G.T., 2023. Techno-economic analysis and life cycle assessment for catalytic fast pyrolysis of mixed plastic waste. Energy Environ. Sci. 16(9), 3638-3653.
[39] Yang, X., Ma, X., Yu, X., Ge, M., 2020. Exploration of strong metal-support interaction in zirconia supported catalysts for toluene oxidation. Appl. Catal., B. 263, 118355-118364.
[40] Yin, Y., Hu, B., Li, X., Zhou, X., Hong, X., Liu, G., 2018. Pd@zeolitic imidazolate framework-8 derived PdZn alloy catalysts for efficient hydrogenation of $CO_2$ to methanol. Appl. Catal., B. 234, 143-152.
[41] Yu, C., Yang, K., Xie, Y., Fan, Q., Yu, J.C., Shu, Q., Wang, C., 2013. Novel hollow Pt-ZnO nanocomposite microspheres with hierarchical structure and enhanced photocatalytic activity and stability. Nanoscale. 5(5), 2142-2151.
[42] Zakaria, A.F., Kamaruzaman, S., Abdul Rahman, N., 2021. Electrospun polyacrylonitrile/lignin/poly (ethylene glycol)-based porous activated carbon nanofiber for removal of nickel (II) ion from aqueous solution. Polymers. 13(20), 3590-3606.
[43] Zeng, R., Wang, K., Shao, W., Lai, J., Song, S., Wang, Y., 2020. Investigation on the coordination mechanism of Pt-containing species and qualification of the alkaline content during Pt/C preparation via a solvothermal polyol method. Chin. J. Catal. 41(5), 820-829.
[44] Zhang, Q., Xu, S., Cao, Y., Ruan, R., Clark, J.H., Hu, C., Tsang, D.C.W., 2022. Sustainable production of gluconic acid and glucuronic acid via microwave-assisted glucose oxidation over low-cost Cu-biochar catalysts. Green Chem. 24(17), 6657-6670.
[45] Zhang, Z., Huber, G.W., 2018. Catalytic oxidation of carbohydrates into organic acids and furan chemicals. Chem. Soc. Rev. 47(4), 1351-1390.
[46] Zhao, X., Wu, G., Zheng, X., Jiang, P., Yi, J.D., Zhou, H., Gao, X., Yu, Z.Q., Wu, Y., 2023. A double atomic-tuned RuBi SAA/Bi@OG nanostructure with optimum charge redistribution for efficient hydrogen evolution. Angew. Chem., Int. Ed. 62(12), e202300879.
[47] Zhou, H., Xu, H., Liu, Y., 2019. Aerobic oxidation of 5-hydroxymethylfurfural to 2,5-furandicarboxylic acid over Co/Mn-lignin coordination complexes-derived catalysts. Appl. Catal., B. 244, 965-973.

Please cite this article as: Hao H., Guo H., Chen B., Smith Jr R.L., Shen F. Sustainable catalytic pathways for biofuel precursors: quantitative conversion of glucose to gluconic acid using Pt-Zn biochar catalyst. Biofuel Research Journal 43 (2024) 2168-2180. DOI: 10.18331/BRJ2024.11.3.3.

**Hengyu Hao** is a graduate student in the Agro-Environmental Protection Institute, Ministry of Agriculture and Rural Affairs: Tianjin, China. Her research interests are green chemistry, biomass resources, sustainability, and platform chemicals. Her research profile can be found at: https://orcid.org/0000-0001-8931-4265

**Prof. Haixin Guo** is a professor at the Agro-Environmental Protection Institute, Ministry of Agriculture and Rural Affairs: Tianjin, China. In 2018, she received a doctorate in environmental science from Tohoku University. She has published more than 60 research articles in peer-reviewed journals and has an h-index of 17 with over 1500 citations. Her research interests are catalysis, green chemistry, valorization of biomass resources, supercritical fluids, ionic liquids, separations engineering, and green chemical processes. Her research profile can be found at: https://orcid.org/0000-0002-0864-5845

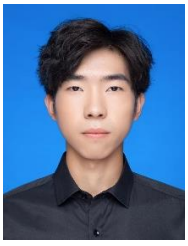

**Bingkun Chen** is a graduate student at the Agro-Environmental Protection Institute, Ministry of Agriculture and Rural Affairs: Tianjin, China. His research interests include electrocatalysis, biomass conversion, dicarboxylic acids, and green chemistry. His research profile can be found at: https://orcid.org/0009-0001-7042-2140

**Prof. Richard Lee. Smith, Jr** is a professor at the Graduate School for Environmental Studies (GP-RSS), Tohoku University, Japan. He obtained his PhD from the Georgia Institute of Technology (USA). He has published more than 300 research articles in peer-reviewed journals and has an h-index of 63 with over 13000 citations. He is an editor for the Journal of Supercritical Fluids and for the Springer-Nature Book Series - Biofuels and Biorefineries. He has research interests in thermodynamics, physical properties, materials, supercritical fluids, environmental applications, and green chemical processes. His research profile can be found at: https://orcid.org/0000-0002-9174-7681

**Prof. Feng Shen** is a professor at the Agro-Environmental Protection Institute, Ministry of Agriculture and Rural Affairs. He obtained his PhD in 2015 in the field of resources and environment from China Agricultural University. He has published more than 65 research articles in peer-reviewed journals and has an h-index of 25 with over 1890 citations. His research focuses on the conversion of biomass to chemicals and materials, and rural environmental management. His research profile can be found at: https://orcid.org/0000-0002-6292-0094

Please cite this article as: Hao H., Guo H., Chen B., Smith Jr R.L., Shen F. Sustainable catalytic pathways for biofuel precursors: quantitative conversion of glucose to gluconic acid using Pt-Zn biochar catalyst. Biofuel Research Journal 43 (2024) 2168-2180. DOI: 10.18331/BRJ2024.11.3.3.

**Supplementary Material**

***Section A.* Turnover frequency (TOF) calculations**

TOFs of glucose for as-synthesized catalysts were calculated by the following steps:

(1) experimental molar content of glucose–reaction time ($t$) curves were fitted with an exponential equation (**Fig. S1**), which was differentiated to give the hydrogenation rate equation ($-dn_{glucose}/dt$). Exponential equations used for Pt-Zn/strawC (**Fig. S1**) are as follows (**Eqs. S1-3**):

$n_{glucose} = 0.41\exp(-t/17.34) - 0.02$ (100 °C), and $n_{glucose} = 0.28\exp(-t/696.32) - 0.0032$ (20 °C) Eq. S1

So, the corresponding differentiated equations are:

$-dn_{glucose}/dt = 0.024\exp(-t/17.34)$ (100 °C) Eq. S2

and

$-dn_{glucose}/dt = 0.028\exp(-t/696.32)$ (20 °C) Eq. S3

(2) initial weight-specific activity ($r_0$) was obtained by substituting zero for $t$ in the hydrogenation rate equation. For Pt-Zn/strawC, $r_0$ was calculated to be 1.18 $mmol_{glucose}\ g_{cat}^{-1}\ min^{-1}$, and 0.02 $mmol_{glucose}\ g_{cat}^{-1}\ min^{-1}$; (3) To ensure the TOF is assessed in the kinetic regime, the TOF was calculated on the basis of the $r_0$ and Pt dispersion using **Equation S4**:

$$\text{TOF} = \frac{\text{Number of glucose molecules converted by catalyst per unit time}}{\text{Number of surface Pt sites}} = \frac{r_0 \times m_{cat} \times N_A}{n_{Pt} \times \text{Pt dispersion} \times N_A}$$

$$= \frac{r_0 \times m_{cat} \times N_A}{(m_{cat} \times \text{Pt loading})/M_{Pt} \times \text{Pt dispersion} \times N_A} = \frac{r_0 \times M_{Pt}}{\text{Pt loading} \times \text{Pt dispersion}}\ (h^{-1}) \quad \text{Eq. S4}$$

where $m_{cat}$, $N_A$, $n_{Pt}$, Pt dispersion, Pt loading, and $M_{Pt}$ are the catalyst mass in each catalytic run, the Avogadro constant, the moles of metallic Pt in each catalytic run, the dispersion of Pt on the catalyst determined by TEM, the loading of Pt on the catalyst determined by ICP–MS, and the molar mass of Pt, respectively. As a result, the TOF of glucose over the as-synthesized Pt-Zn/strawC catalyst was calculated to be 4819 $h^{-1}$ (100 °C) and 82 $h^{-1}$ (20 °C).

**Section B. Computational methods**

All spin-polarized calculations on catalysts were performed using the Vienna ab initio Simulations Package (VASP) based on density functional theory (DFT) simulations. The Perdew–Burke–Enzerhof (PBE) method, projector augmented wave (PAW) method, and a plane-wave basis set with a cut-off energy of 400 eV were employed for optimizing the geometrical configurations of the catalyst. To study the adsorption or desorption on the catalyst surfaces, the slab models were periodically repeated in the z direction perpendicular to the surface and separated from their images by a vacuum gap larger than 15 Å. The Gamma point was utilized to sample reciprocal space. Geometry relaxation was performed with a convergence criterion of 0.05 eV $Å^{-1}$, and the energy convergence threshold was $1 \times 10^{-4}$ eV. The dispersion interaction was described with Grimme's DFT-D3 correction. The adsorption and desorption energies were estimated using **Equations S5** and **6**:

$$E_{ads} = E(\text{slab} + \text{adsorbate}) - E(\text{slab}) - E(\text{adsorbate}) \quad \text{Eq. S5}$$

$$E_{des} = -(E(\text{slab} + \text{desorbate}) - E(\text{slab}) - E(\text{desorbate})) \quad \text{Eq. S6}$$

where E(slab + adsorbate), E(slab), and E(adsorbate) represent the energies of species adsorbed (desorbed) on the surface, the bare surface, and the matter-phase molecule, respectively.

Please cite this article as: Hao H., Guo H., Chen B., Smith Jr R.L., Shen F. Sustainable catalytic pathways for biofuel precursors: quantitative conversion of glucose to gluconic acid using Pt-Zn biochar catalyst. Biofuel Research Journal 43 (2024) 2168-2180. DOI: 10.18331/BRJ2024.11.3.3.

**Table S1.**
ICP-MS results of as-samples.

| Entry | Catalyst | Pt loading (mg/g) | Zn loading (mg/g) |
|---|---|---|---|
| 1 | Pt-Zn/strawC | 17.8 | 4.4 |
| 2 | Zn/strawC | - | 16.9 |
| 3 | Pt/strawC | 12.1 | - |

**Table S2.**
Initial molar ratio of metal and XPS elemental analysis of sample surface.

| Entry | Catalyst | Initial Molar Ratio | Surface Elemental Composition | | | |
|---|---|---|---|---|---|---|
| | | Pt:Zn | Pt/Zn molar ratio | $O_{O\text{-}H}/O_{total}$ (%) | $O_{ads}/O_{total}$ (%) | $O_{Latt}/O_{total}$ (%) |
| 1 | Pt-Zn(1:3)/strawC | 1:3 | 0.4 | 35.7 | 33.1 | 31.2 |
| 2 | Pt-Zn(1:1)/strawC | 1:1 | 1.0 | 34.3 | 32.8 | 32.9 |
| 3 | Pt-Zn/strawC | 1:6 | 1.1 | 35.0 | 33.1 | 31.9 |
| 4 | Pt/strawC | - | - | 30.6 | 39.7 | 29.7 |
| 5 | Zn/strawC | - | - | 34.7 | 33.5 | 31.8 |
| 6 | Spent Pt-Zn/strawC | 1:6 | 4.1 | 37.6 | 32.9 | 29.5 |

**Table S3.**
Process, economic, energy, and environmental indicators of heterogeneous catalysts for oxidation of glucose*.

| Entry | Catalyst | Process efficiency | Catalyst Cost | Energy Consumption | Oxidant Cost | Environmental Benefits | Cycling Performance | Ref. |
|---|---|---|---|---|---|---|---|---|
| 1 | CuBC600N | 2 | 5 | 1 | 2 | 1 | 3 | Zhang et al. (2022) |
| 2 | Pd/CNT-N | 5 | 2 | 5 | 1 | 3 | 5 | Li et al. (2021) |
| 3 | Pd/C | 4 | 4 | 5 | 3 | 4 | 4 | Liu et al. (2018) |
| 4 | $Ni_{ED}$/XC72 | 1 | 4 | 3 | 5 | 2 | 1 | Medrano-Banda et al. (2024) |
| 5 | Pt/def-$TiO_2$ | 3 | 3 | 4 | 5 | 1 | 5 | Tian et al. (2023) |
| 6 | Pt-Zn/strawC | 5 | 4 | 5 | 5 | 5 | 4 | **Present Study** |

* *Note:* The number of each indicator is based on the following data, and the maximum score is 5 points.
The process efficiency of catalysts was decided by the yield of sugar acids, which were 69.7, 98.3, 98, 20, 84.3, and 99.9%, respectively.
The energy consumption, oxidant cost, and environmental benefits are shown in **Table 1**.
The catalyst cost is evaluated based on the raw materials in its preparation, such as the type of metal and the support.

Please cite this article as: Hao H., Guo H., Chen B., Smith Jr R.L., Shen F. Sustainable catalytic pathways for biofuel precursors: quantitative conversion of glucose to gluconic acid using Pt-Zn biochar catalyst. Biofuel Research Journal 43 (2024) 2168-2180. DOI: 10.18331/BRJ2024.11.3.3.

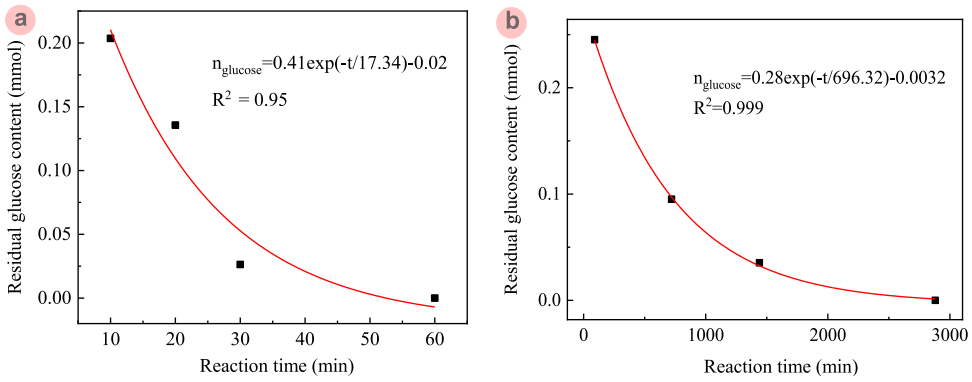


**Fig. S1. (a-b)** Fitting results of molar content of glucose–reaction time curves over the as-synthesized Pt-Zn/strawC catalyst (*Reaction conditions:* 0.05 g of glucose, 0.02 g of catalyst, and 5 mL of $H_2O$). **a:** $O_2$ partial pressure of 1 MPa, temperature of 100 °C, and stirring rate of 800 rpm; **b:** air pressure, temperature of 20 °C, and stirring rate of 500 rpm.

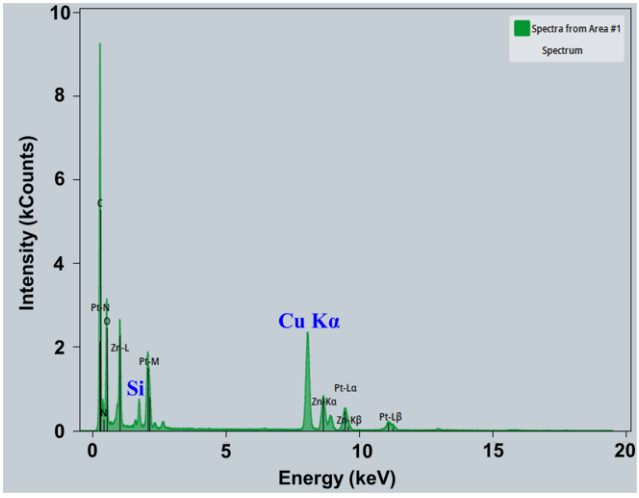


**Fig. S2.** TEM-EDX element atomic percentages of Pt-Zn/strawC.

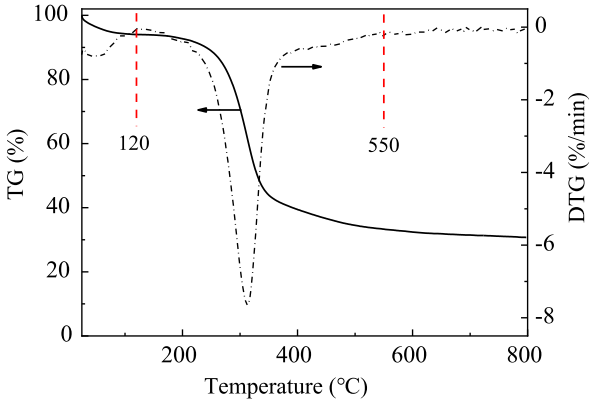


**Fig. S3.** TG-DTG curves of rice straw after ball milling.

Please cite this article as: Hao H., Guo H., Chen B., Smith Jr R.L., Shen F. Sustainable catalytic pathways for biofuel precursors: quantitative conversion of glucose to gluconic acid using Pt-Zn biochar catalyst. Biofuel Research Journal 43 (2024) 2168-2180. DOI: 10.18331/BRJ2024.11.3.3.

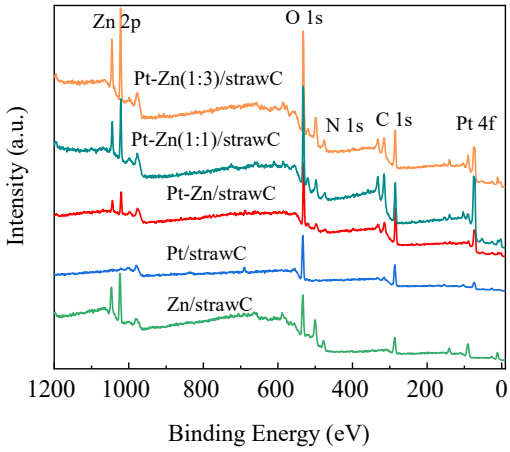


**Fig. S4.** XPS survey spectra of as-prepared catalysts.

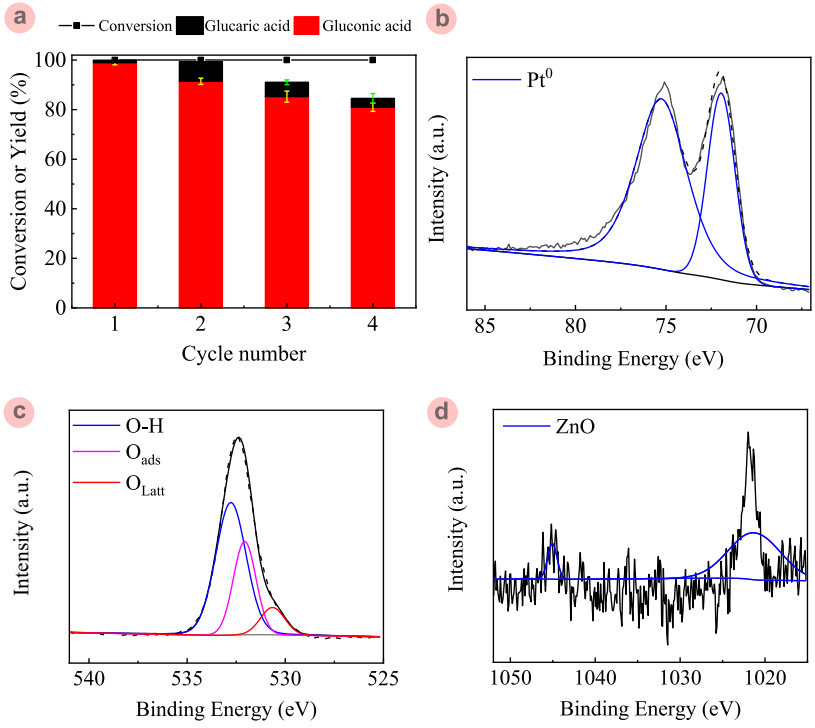


**Fig. S5.** Oxidation of glucose to gluconic acid over Pt-Zn/strawC catalyst: **(a)** recycling trials (Reaction conditions: 0.05 g of glucose, 0.02 g of catalyst, 5 mL of water, at 20 oC, and after 72 h reaction time). XPS spectra of spent Pt-Zn/strawC catalyst: **(b)** Pt 4f, **(c)** O 1s, and **(d)** Zn 2p.

Please cite this article as: Hao H., Guo H., Chen B., Smith Jr R.L., Shen F. Sustainable catalytic pathways for biofuel precursors: quantitative conversion of glucose to gluconic acid using Pt-Zn biochar catalyst. Biofuel Research Journal 43 (2024) 2168-2180. DOI: 10.18331/BRJ2024.11.3.3.

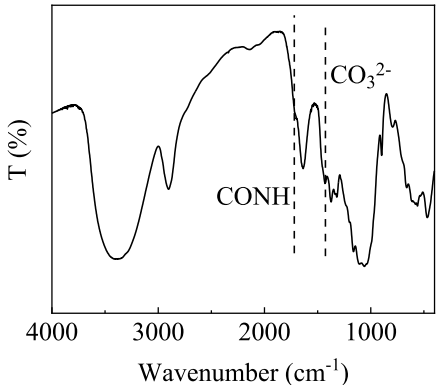


**Fig. S6.** FTIR spectra for spent Pt-Zn/straw.

## References

[1] Li, Z., Li, D., Lan, W., Li, X., Wan, X., Sun, R., Liu, C., Peng, X., 2021. Highly selective oxidation of monosaccharides to sugar acids at room temperature over palladium supported on surface functionalized carbon nanotubes. Green Chem. 23(18), 7084-7092.

[2] Liu, A., Huang, Z., Wang, X., 2018. Efficient oxidation of glucose into gluconic acid catalyzed by oxygen-rich carbon supported Pd under room temperature and atmospheric pressure. Catal. Lett. 148(7), 2019-2029.

[3] Medrano-Banda, A., Ginoux, E., Faverge, T., Oshchepkov, A., Bonnefont, A., Chatenet, M., Coutanceau, C., Kéranguéven, G., Cognet, P., Savinova, E., 2024. Electrochemical oxidation of glucose in alkaline environment-a comparative study of Ni and Au electrodes. Electrochim. Acta. 487, 144159.

[4] Tian, Z., Da, Y., Wang, M., Dou, X., Cui, X., Chen, J., Jiang, R., Xi, S., Cui, B., Luo, Y., Yang, H., Long, Y., Xiao, Y., Chen, W., 2023. Selective photoelectrochemical oxidation of glucose to glucaric acid by single atom Pt decorated defective $TiO_2$. Nat. Commun. 14(142).

[5] Zhang, Q., Xu, S., Cao, Y., Ruan, R., Clark, J.H., Hu, C., Tsang, D.C.W., 2022. Sustainable production of gluconic acid and glucuronic acid *via* microwave-assisted glucose oxidation over low-cost Cu-biochar catalysts. Green Chem. 24(17), 6657-6670.

Please cite this article as: Hao H., Guo H., Chen B., Smith Jr R.L., Shen F. Sustainable catalytic pathways for biofuel precursors: quantitative conversion of glucose to gluconic acid using Pt-Zn biochar catalyst. Biofuel Research Journal 43 (2024) 2168-2180. DOI: 10.18331/BRJ2024.11.3.3.